Transfer of Posture and Kinematics from Pre-Crash Madymo HBM to In-Crash VIVA+ Simulations for Holistic Vehicle Safety Analyses

Desiree Kofler, Niklas Fahse, Felix Ressi, Jörg Fehr, Corina Klug

Abstract Active human body models (HBMs) enable the investigation of a collision as a single continuous sequence covering the pre- and in-crash phases. However, their computational cost makes them less suited for large parameter spaces. This study presents an approach for transferring information from multi-body (MB) to finite element (FE) HBMs, while preserving kinetic energy at t_0.

A common basis between the MB and FE HBM was established by matching anthropometries, initial poses, and landmarks. To preserve kinetic energy at collision, landmark kinematics, including velocities, were applied. The influence on in-crash kinematics and injury risk was evaluated against only positioning landmark coordinates.

Three options were compared: (A) the landmarks were pulled to their static target positions using spring elements and nodal velocities were set to zero; (B) based on the positioning method (A), body segment velocities were set to the corresponding values; and (C) the motion of the landmarks was directly prescribed based on velocity data from their respective MB-HBM counterparts.

Occupant kinematics were successfully transferred to the FE HBM model. The results highlight that, depending on the pre-crash scenario, omitting velocities can lead to substantial differences in in-crash kinematics and injury risk metrics. Hence, no clear trend across scenarios could be identified.

Keywords Finite element simulation, Human body models, Multi-body simulation, Occupant protection, Pre-crash kinematics.

I. INTRODUCTION

The importance of considering human behaviour in pre-crash manoeuvres when it comes to finite element (FE) simulation using human body models (HBMs) has been highlighted by various studies. Braking or evasive manoeuvres influence the occupant's state at the time of crash (t_0), such as position, posture and relative velocities [1]. Deviations in these initial conditions affect the occupant behaviour during the crash, which may lead to different injury outcomes [2-9].

There are three groups of methods for considering the pre-crash movement of the occupant for in-crash simulations. The first group models both the pre- and in-crash phases into a single simulation [8][10]. The main benefit of this method is the seamless transition between the pre- and the in-crash phases, ensuring that conditions such as relative velocities and material strains established during pre-crash movement are preserved. However, realistic prediction of occupant behaviour in the pre-crash phase requires the application of HBMs with active muscle control (A-HBMs). Whether the braking or evasive manoeuvre is initiated by the driver or by active safety systems, the pre-crash phase can last several seconds. A-HBMs are computationally expensive, so applying them to simulations over such a long period is computationally very demanding [3].

Efforts have been made to introduce simplified and fast A-HBMs to reduce the processing time of pre-crash simulations [5]. The simplification of such models comes at the expense of their ability to reproduce the injury mechanisms in the in-crash phase. Therefore, the second group of methods uses two separate simulations for the pre- and the in-crash phases. Active but simplified HBMs are used to predict the pre-crash behaviour of the occupant, while detailed HBMs facilitate injury assessment during the in-crash phase [1-2][4-5][7]. This method necessitates the transfer of the state at the end of the pre-crash phase to the initial state of the in-crash phase. The accuracy of the replicated initial occupant conditions depends on the amount and type of information transferred. This transfer of the posture can be managed by simply replacing the nodal coordinates with special

D. Kofler (desiree.kofler@tugraz.at, +43 316 873 30350) is a Researcher, F. Ressi is a Senior Project Scientist and C. Klug is an Associate Professor at the Vehicle Safety Institute, Graz University of Technology, Austria. N. Fahse is a Research Associate and Doctoral Student and J. Fehr is a Professor at the Institute of Engineering and Computational Mechanics, University of Stuttgart, Germany.

morphing tools [1], which require the HBMs used in the pre-crash and the in-crash phases to share the same node IDs. An alternative can be to position the in-crash HBM via a dedicated pre-simulation to the desired position. Velocities can be transferred by applying additional initial velocities to individual body regions of the positioned model prior to the crash [11]. But the separation between pre- and in-crash simulations lacks the transfer of initial strains in soft tissue and ligaments of the HBM [4]. Additionally, the positioning procedure and velocity transfer must be performed separately for each pre-crash scenario.

The third group applies a short HBM positioning phase prior to the in-crash phase in the same simulation run to mimic diverse pre-crash scenarios as well as the preservation of initial strain conditions. Guiding the HBM in a marionette-like fashion to the desired target position is a commonly used method [7]. The replication of the t_0 kinematics is enhanced by additionally applying initial velocities to the HBM after the pre-crash phase [12].

In summary, common methods already replicate the HBM posture, initial strains and velocities in different combinations. To the authors' knowledge, no investigation has been conducted to analyse the effect of considering the occupant's movement throughout the entire pre-crash phase rather than focusing solely on the final position. Therefore, this study investigates an approach that focuses on the transfer of the pre-crash posture based on velocity-dependent landmark kinematics. The HBM positioning is done in a shortened pre-crash phase and is based on an adapted marionette method that controls the movement in a velocity-based rather than a displacement-based manner. This study tests the hypothesis that positioning the HBM by applying time-dependent velocities to anatomical landmarks will yield a more accurate representation of the posture after the pre-crash phase than conventional displacement-based approaches. The magnitude of this potential improvement in posture fidelity remains to be quantified.

To investigate this matter, a new approach was developed, combining multi-body (MB) and FE simulation. MB models operate with simplified models that focus on kinematics and kinetics, making them ideal for long-duration phases. In-crash phases, where detailed loads and injury metrics are of interest, are commonly evaluated using more complex FE models. A tool to transfer the pre-crash posture and kinematics derived from MB simulation to FE simulations was introduced. The effect of the new approach is determined by comparing the in-crash kinematics and injury metrics with those obtained using existing methods.

II. METHODS

A brief description of the general approach of the method is provided, followed by a detailed description of each subsection. Fig. 1 shows the method, which combines MB simulations (blue) and FE simulations (red) with the developed posture and kinematics transfer tool (yellow).

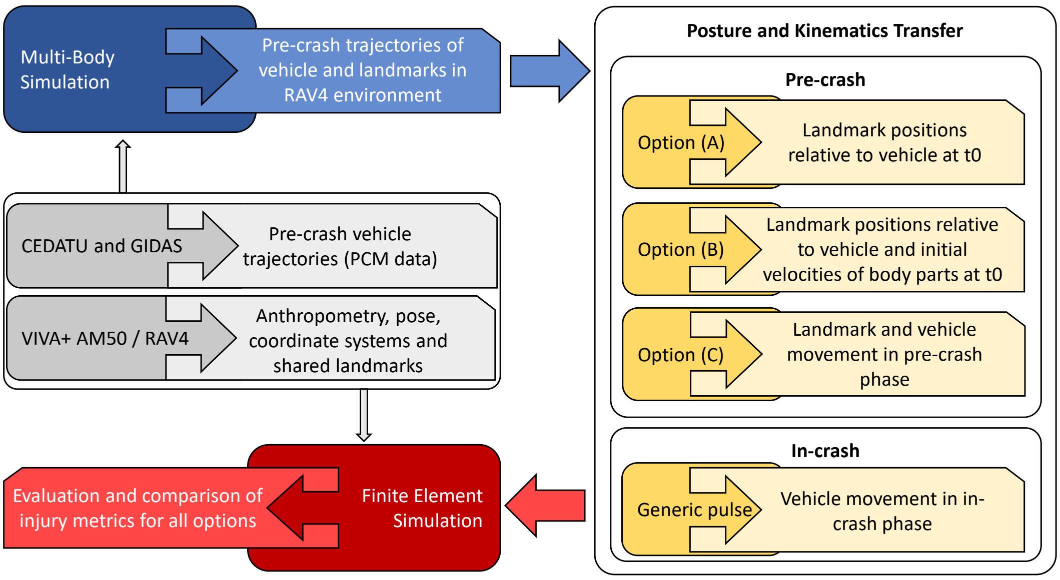

Fig. 1. Posture and kinematics transfer combining multi-body and FE simulations.

Pre-crash vehicle trajectories reconstructed using PC-Crash [13] based on accident cases from the CEDATU [14] and GIDAS [15] databases served as input for the MB simulations. In-crash FE simulations were conducted considering the pre-crash phase determined in the MB simulations. The posture and kinematics transfer links the two simulation tools and processes the pre-crash data from MB to be applied in the FE simulation according to the three different options, (A), (B) and (C). The tool involves handling and transmitting data from the MB model to the FE model, as well as preparing the FE input decks in the correct format. The comparison of the in-crash behaviour of all options facilitated the evaluation of the influence of the corresponding positioning method.

Multi-Body Simulations

Multi-body pre-crash simulations were conducted using Simcenter Madymo R2020.1. The simulations were conducted using the Madymo 50th percentile male Active Human Model (AHM-50M), representing a 50th percentile male, parameterised from the RAMSIS database, with facet-based contact definitions in seated configuration ("h_act50fc_sitting", Madymo R7.8). The model represents a detailed multi-body occupant model including articulated spinal segments, deformable thorax representation, ellipsoid and facet contact interfaces, and Hill-type active muscle controllers for human body dynamics. To ensure consistency with the environment of the subsequent in-crash FE simulations and to reflect automated driving use cases, a passenger-side occupant configuration was implemented. For this purpose, the driver-side OSCCAR model [8] was transformed into a passenger model by mirroring the seat and load application points, mirroring the relevant FE nodes of the belt anchorage system, and defining a new belt-positioning procedure in Madymo to obtain a realistic belt routing over the passenger-side A-HBM.

The A-HBM was visually adjusted to match the posture of the HBM VIVA+ 50M used for the FE simulations. It comprises 190 bodies (182 rigid, 8 flexible) and 52 joints, based on a facet-based multi-body formulation with rigid surface FE technology, and includes detailed musculature with 68 pairs of neck muscles. The posture stabilisation system comprises a set of reflex controllers designed to reproduce human neuromuscular responses over a range of control bandwidths. Active neuromuscular control was enabled for the neck, spine, shoulders, elbows, hips, and knees using the built-in Madymo active control framework. The controller architecture incorporates reaction-time-based feedback control, muscle activation dynamics, co-contraction functionality, and local body reference tracking for head stabilization relative to the upper thoracic spine (T1 reference body). The controllers actuate the musculature of the head and neck, upper extremities, and lower extremities, while spinal stabilisation is represented using distributed torque actuators along the vertebral joints. Joint posture is regulated using PID-based feedback controllers, and neck muscle co-contraction is included to reproduce realistic pre-impact occupant kinematics. In the present study, a reaction time of 100 ms was applied and all regional activation controllers were enabled.

The Madymo Active Human Model (AHM-50M) employed in this study has previously been evaluated for low-severity occupant motion and pre-crash kinematics using volunteer-based experimental conditions reported in the literature and within the Madymo model documentation [16]. The posture stabilisation system incorporates neuromuscular reflex controllers intended to reproduce characteristic human responses such as head stabilisation, bracing, and postural control during vehicle manoeuvres.

Validation of active human body models remains an active research field and includes investigations on control strategies, muscle activation behaviour, and inter-subject human variability using volunteer sled tests, real-vehicle experiments, and driver-in-the-loop simulator studies. Within the present research project, dedicated validation activities are currently being conducted using a novel low-g sled-test setup [17] with rotated occupant configurations to investigate active occupant behaviour during pre-crash manoeuvres.

A recent study by Diederich *et al.* [18] demonstrated the validation and calibration of Active Human Models using volunteer-based kinematic corridors obtained from OM4IS and UMTRI experiments under pre-crash manoeuvres. In this context, the AHM parameters were optimised using multi-objective optimisation and CORA-based correlation methods to reproduce occupant kinematics in rotated seating configurations and different restraint conditions [18].

Nevertheless, the focus of the present work is not the development or validation of the A-HBM itself. Instead, this study investigates the transfer of pre-crash occupant states into in-crash simulations and evaluates the influence of active pre-crash occupant motion on subsequent crash loading and injury prediction workflows. For this purpose, the A-HBM is considered a validated biomechanical reference framework for representing active occupant behaviour under pre-crash loading conditions.

Central to the simulation is the synthesis of realistic vehicle acceleration inputs, which dictate the boundary conditions for the occupant model. Here, Macaulay functions – piecewise linear functions capable of activating terms at specified times – were utilised to generate parametric acceleration pulses that replicate typical pre-crash events. These functions allow for the concise definition of discontinuous or time-varying loads, making them ideal for modelling the abrupt onset of braking or steering inputs. From the CEDATU reconstructions, multi-axis acceleration pulses were clustered using k-means clustering to identify representative pre-crash motion patterns. One cluster characterised by strongly coupled longitudinal and lateral accelerations was selected as representative. Acceleration pulses reconstructed from GIDAS UTYP 141 [3] (run-off-road accident) were subsequently compared with the centroid of this representative cluster. Such pulses form the baseline of our approach. Two generic pulse types were synthesised to represent pre-crash scenarios: (i) a pure braking pulse, characterised by rapid deceleration to simulate emergency braking on straight rural or highway segments, referred to as scenario *Brake*; and (ii) a combined braking and steering pulse, which introduces a lateral acceleration component to mimic evasive manoeuvres, referred to as scenario *Brake & Steer*. These pulses correspond to scenarios identified by the clustering of accidents on curved rural roads and highway entry or exit ramps, which can generate coupled longitudinal-lateral vehicle accelerations. The braking pulse typically features a step from zero to a peak deceleration of 12 m/s² followed by a sustained plateau, while the combined pulse overlays a step-like lateral acceleration of 6 m/s² to simulate steering-induced yaw. These synthesised pulses serve as the primary inputs for the vehicle dynamics model, ensuring that the simulated pre-crash motions are both realistic and reproducible, and are plotted in Fig. 2 in the upper row (black).

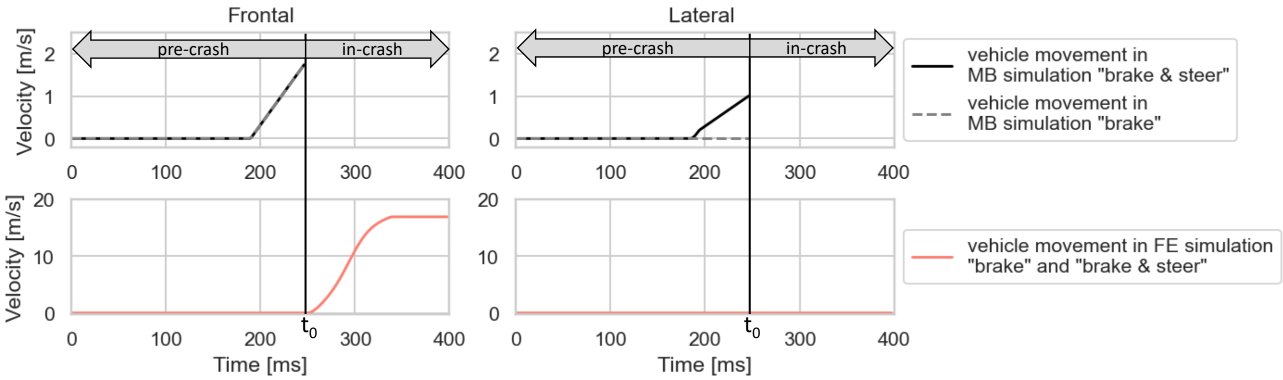

Fig. 2. Vehicle movement in MB pre-crash simulation for the scenarios *Brake* and *Brake & Steer* (top) and vehicle movement in FE pre- and in-crash simulation (bottom).

To translate the longitudinal and lateral accelerations into a full six-degree-of-freedom vehicle motion, a unicycle model was employed [19]. This simplified kinematic model approximates the vehicle as a single rigid body moving in the plane, with its heading angle $\psi(t)$ determined by the ratio of lateral acceleration $a_y(t)$ to the longitudinal velocity $v_x(t)$, yielding the yaw rate $\dot{\psi}(t) = \frac{a_y(t)}{v_x(t)}$.

The yaw angle $\psi(t)$ is then obtained through numerical integration of the yaw rate over time. This approach ensures that the vehicle's rotational motion is consistently coupled with its translational dynamics, providing a physically coherent input for the multi-body occupant model. The unicycle model's simplicity and computational efficiency make it particularly suitable for pre-crash simulations, where the focus is on capturing the essential dynamics of vehicle motion without the complexity of full vehicle dynamics models.

The workflow for preparing the MB models is shown in Fig. 3.

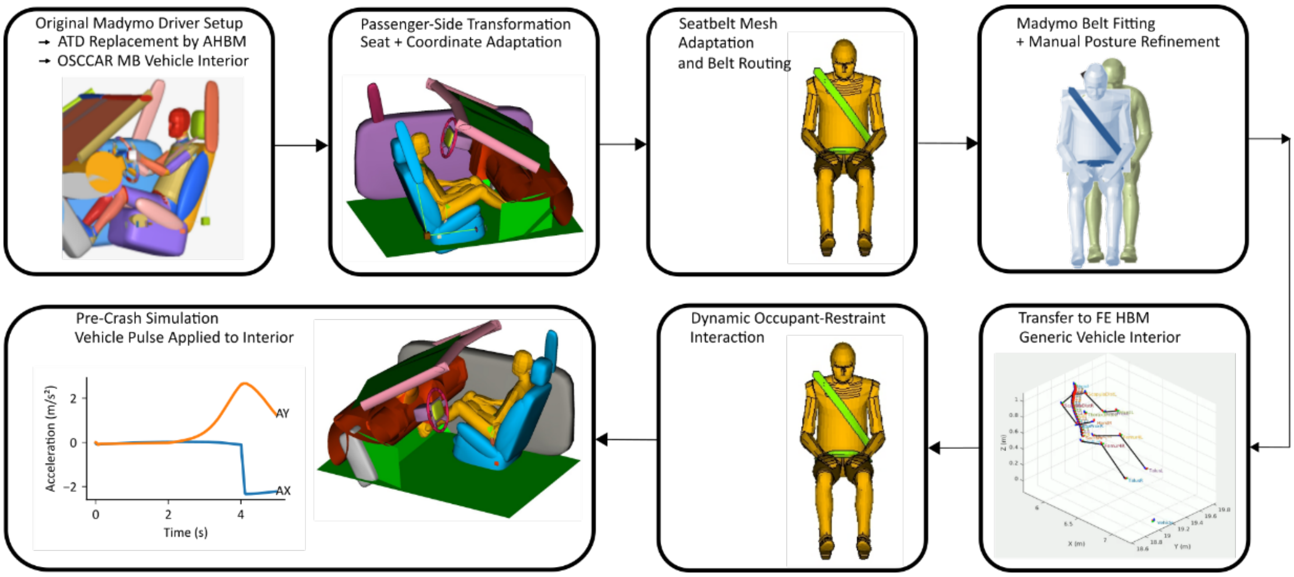

Fig. 3. Flowchart illustrating the adaption of the original Madymo driver model to the passenger side model used in the FE simulations.

The pre-crash simulations were based on the original driver-side Madymo configuration derived from the highly parameterised generic multibody vehicle interior model developed within the OSCCAR project together with the Simcenter Madymo frontal passenger application model. In the original setup, the ATDs were replaced by the Active Human Body Model (A-HBM).

Since the original Madymo configuration was not directly compatible with the finite element Generic Vehicle Interior (GVI) environment used for the subsequent in-crash simulations, several adaptation steps were required. In particular, differences in coordinate systems, unit systems, restraint definitions, and initial occupant positions between the multibody and finite element environments had to be resolved to ensure a consistent transfer of the occupant state.

The occupant model was transferred from the driver side to the passenger side by mirroring and adapting the seat environment, restraint anchor locations, and associated coordinate systems. As no dedicated passenger-side belt mesh was available in the original model, the existing driver-side belt mesh was geometrically mirrored and integrated into an updated XML restraint-definition file for the passenger-side configuration.

Subsequently, the belt anchor definitions and belt-routing parameters were adapted, and the Madymo belt-fitting tool was used to obtain anatomically realistic belt routing over the thorax and pelvis of the A-HBM. Following the automatic belt-fitting process, manual posture refinements were performed, including adjustments of the upper extremities, lower extremities, and shoulder posture, as well as the removal of local penetrations between occupant, seat, and restraint components. A comparison of the resulting belt routing in the multibody and finite element environments is provided in the Appendix (Figs. C8, C9), showing front and side views with the belt anchor locations highlighted.

The belt-fitting procedure was completed prior to the dynamic pre-crash simulation. During the subsequent pre-crash phase, reconstructed GIDAS acceleration pulses were applied to the vehicle interior reference frame rather than directly to the occupant model. This approach ensures physically consistent inertial interaction between occupant, restraint system, and vehicle environment during the manoeuvre. Direct acceleration of the occupant model without corresponding vehicle and restraint motion would not reproduce realistic belt interaction and relative occupant-to-interior kinematics.

Throughout the pre-crash simulation, the restraint system remained fully coupled to the occupant model. The belt anchor locations were fixed relative to the vehicle structure, while belt forces, belt tension development, and occupant kinematics evolved dynamically due to the relative motion between occupant and vehicle interior. Consequently, belt preload at crash initiation emerged naturally from the simulated pre-crash occupant motion and restraint interaction rather than from predefined initial conditions.

After completion of the pre-crash phase, the full occupant kinematics, joint states, and associated coordinate systems were extracted and transferred consistently to the finite element in-crash simulation environment. The primary objective of this workflow was not the exact replication of local belt stresses between the multibody and finite element environments, but rather the transfer of a physically plausible pre-crash occupant state into the subsequent high-fidelity in-crash simulation for injury prediction assessment.

The simulation produces continuous three-dimensional trajectories and velocities for the anatomical landmarks – including the head centre, sternum, T8 vertebra, and bilateral hip centres – as well as for eight body regions, such as the head-neck complex, thorax, pelvis, and limbs. The anatomical landmarks and body region definitions are derived from the detailed FE HBM used for subsequent in-crash analysis. All joint positions were automatically extracted from input and output files by parsing both HDF5 result files and simulation input files. The workflow is shown in Fig. 4.

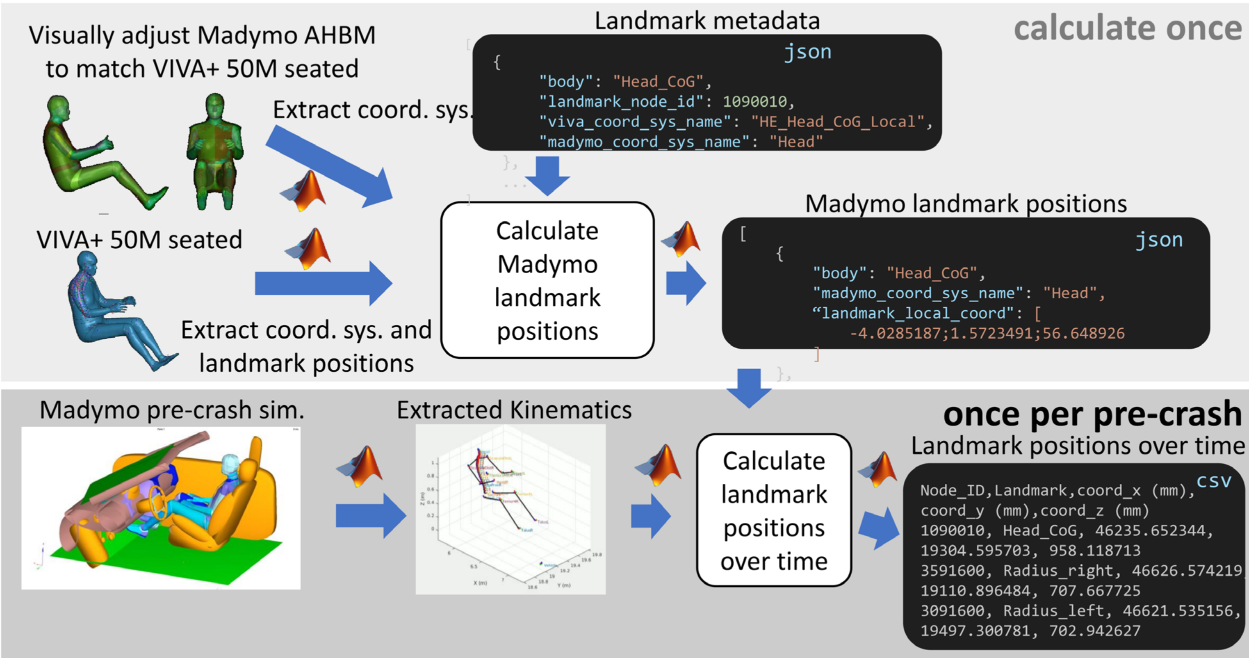

Fig. 4. Workflow of the positioning of the MB model and the extraction of the kinematics for the subsequent FE simulation.

This integrated workflow bridges the gap between pre-crash vehicle dynamics and in-crash occupant response, enabling a comprehensive assessment of occupant movement. The use of Macaulay functions for pulse synthesis ensures that the acceleration inputs are both flexible and precise, while the unicycle model provides a robust method for converting these inputs into realistic vehicle motions.

Posture and Kinematics Transfer

Python scripts were developed to read the CSV files obtained from the MB simulation, apply calculation routines, and write input decks in LS-Dyna format. The effects of considering the HBM behaviour during the pre-crash phase on the in-crash response were determined by comparing three different methods. Fig. 5 illustrates the working principles of the three approaches.

For all three options, a single continuous simulation was set up with no dynamic relaxation applied. Options (A) and (B) do not take pre-crash kinematics into account, focusing solely on the HBM posture at t_0. To achieve the desired HBM posture, the landmarks were moved to the target coordinates in a marionette-like fashion. The positioning beams were released at the transition to the in-crash phase, allowing the landmarks to move freely. Option (A) differs from option (B) in that the HBM velocities were set to zero at the onset of the load; in option (B), each body region was initialised with an initial translational velocity prior to the crash. In both approaches, the velocity application for the in-crash-phase was performed using the *INITIAL_VELOCITY_GENERATION and *INITIAL_VELOCITY_GENERATION_START_TIME keywords.

Option (C) considers the entire path that the landmarks follow during the pre-crash phase. The landmarks were given translational and rotational velocity-based motion control in a shortened pre-crash phase to move the HBM to the desired posture and position. This phase lasts 250 ms, regardless of the length of the input pre-crash pulse. To achieve the correct target HBM posture, the velocities must be scaled by the inverse of the scale factor applied to the time channel.

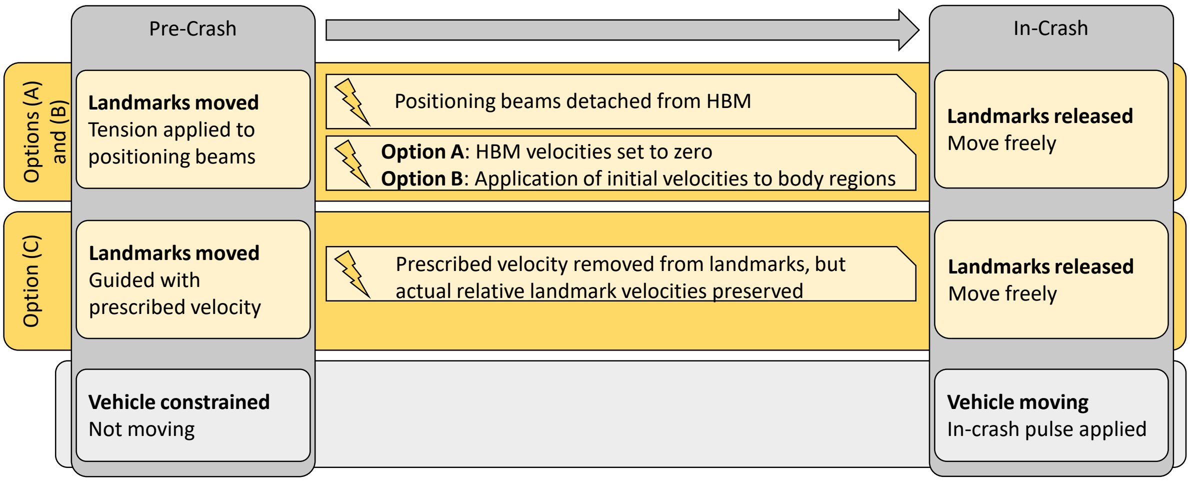

Fig. 5. Posture and kinematics transfer for options (A), (B) and (C).

As this would result in velocities that are too high at t_0, scaling was only applied to 99% of the original MB pre-crash duration, which is 623.7 ms. The velocities then drop to a normal level within the final 1% of the pre-crash phase, which is 6.3 ms. This method benefits from decreased pre-crash simulation time in conjunction with correct nodal velocities of the entire HBM at t_0. To prevent the HBM soft tissue from deforming due to inertia induced by high velocities, damping was applied during the pre-crash phase. The damping factor was linearly reduced to zero within the final 5% of the pre-crash duration and remained at zero throughout the in-crash phase.

The outcomes of positioning options (A) and (B) are unaffected by the length of the pre-crash phase. All that is required is sufficient time for the positioning beams to fully contract. Nevertheless, the same damping was applied to options (A) and (B) as well. The vehicle movement is the same for all three options: stationary in the pre-crash phase and moving according to the crash pulse in the in-crash phase.

In summary, the following logic was applied for options (A) and (B):

- Positioning phase: 250 ms
  - No vehicle movement
  - Positioning of HBM landmarks using positioning beams (marionette method)
  - Damping applied (linearly reduced to zero within the final 12.5 ms)
- At transition point:
  - Positioning beams released
  - Option (A): all velocities set to zero
  - Option (B): initial translational velocities applied to body regions based on MB simulation
- In-crash (150 ms):
  - Vehicle movement (based on crash pulse)
  - No damping

For option (C), the logic was slightly different:

- Positioning phase: 250 ms
  - No vehicle movement
  - Positioning of HBM using velocity-based motion control for each landmark (translational & rotational)
  - Scaled velocities applied (to shorten pre-crash phase duration) for 99% of positioning phase
  - Prescribed velocities reduced to normal level in the final 1% of positioning phase
  - Damping applied (linearly reduced to zero within the final 12.5 ms)
- At transition point: landmarks are allowed to move freely (end of velocity-based motion control)
- In-crash (150 ms):
  - Vehicle movement (based on crash pulse)
  - No damping

Finite Element Simulation

The influence of different positioning methods was evaluated using simulations with a parametric FE vehicle model developed by Boyle *et al.* [20]. The generic vehicle (GVI) can be morphed to various vehicle geometries, whereby selected vehicle geometries have been calibrated against US NCAP tests. The GVI morphed and calibrated for the Toyota RAV4 was chosen and adapted to be compatible with the content of the LS-Dyna file generated from the posture transfer tool. Furthermore, the GVI was reduced to only contain essential equipment for the simulation of the passenger side. The removal of seat, belt and airbags on the driver side helped to decrease the simulation time. The model includes a parameterised definition of a generic crash pulse [21]. The parameters replicating the crash pulse of the full-width frontal US NCAP test with a Toyota RAV4 are provided in the model and were adopted to represent the in-crash pulse for both pre-crash scenarios. The consequential vehicle movement is shown in Fig. 2 in red. The parameters forming the in-crash pulse are provided in TABLE AI in the Appendix.

The seated model of VIVA+ v2.0.1 50M [22-23] was positioned with the hands on the thighs via a separate positioning pre-simulation. No adaptations to the posture were done besides the positioning of the upper extremities. The passenger seat was moved to the mid/mid position of the Toyota RAV4 and deformed to match the geometry of the seated HBM. An initial foam reference geometry was implemented to reproduce the pre-stressed seat foam. The 3-point belt included in the GVI was fitted.

Fifteen landmarks were used to move the HBM to the desired position for all three positioning options. An additional node was introduced for each landmark and constrained to the part of the respective bone. The connection between the nodes and the corresponding parts was realised using fixation beams, as shown for the head centre of gravity (CoG) in Fig. 6 (left). These rigid beams are only active during the pre-crash phase and are deleted when the in-crash pulse begins.

Fixation beams for one landmark covering multiple bones were installed for the thorax. To avoid local deformation of the sternum, the landmark *sternum mid* was connected to the sternum but also to the most anterior part of each cortical rib (see Fig. 6 *right*). The landmark on the *T8 centre* was also constrained additionally to all other thoracic vertebrae to prevent potential relative movement of the T8 vertebra with respect to the adjoining vertebrae.

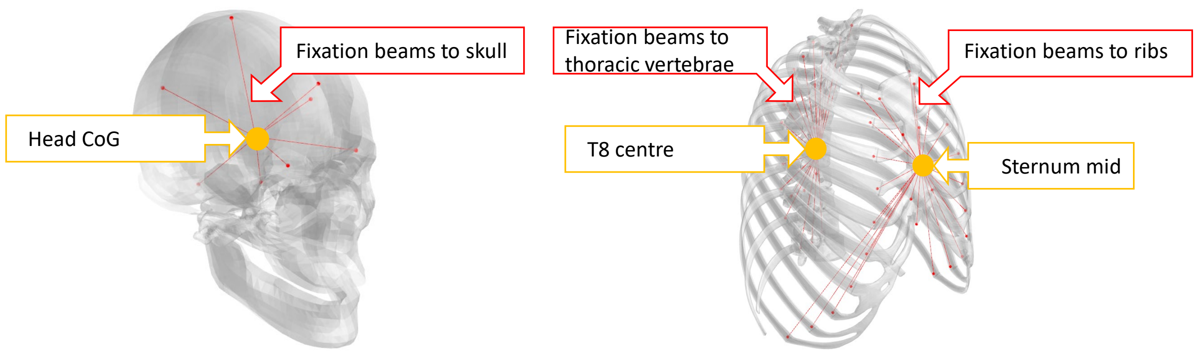

Fig. 6. Fixation beams connecting landmark *head CoG* to the skull (*left*) and extended fixation beams for thoracic landmarks (*right*).

Positioning options (A) and (B) use positioning beams to move the landmarks to their target position, as shown in Fig. 7 (*left*). Each beam connects a landmark node with a node located at the corresponding target coordinates. The target nodes were rigidly fixed to the vehicle. By applying a tension force on each beam, the landmark is dragged to the target node position. Since the fixation beams are deleted when the crash pulse is applied, the positioning beams are detached from the HBM and do not influence the HBM's behaviour during the in-crash phase.

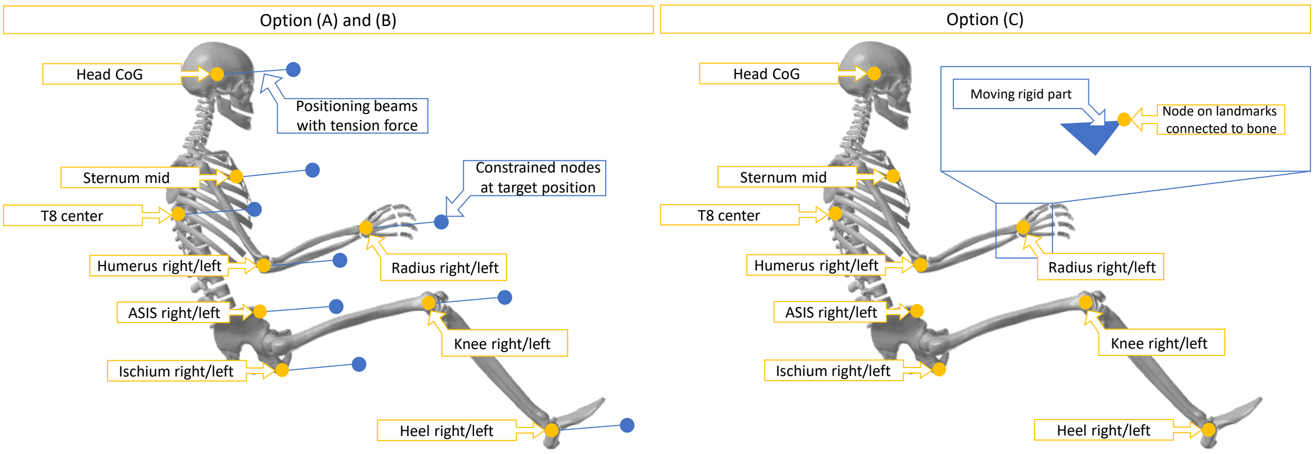

Fig. 7. HBM positioning methods for options (A) and (B) (*left*) and option (C) (*right*).

Options (A) and (B) differ from the time of onset of the crash pulse. The initial velocity of the HBM is set to zero in option (A), whereas initial velocities are applied for each body region in option (B). The body regions divide the HBM into head, neck, thorax, left and right upper arm, left and right lower arm including the hand, pelvis, left and right upper leg, left and right lower leg, and left and right foot. The initial translational velocities at the centre of gravity of each body region were derived from the MB simulation and applied to the part sets forming the body regions for the VIVA+ model.

Instead of focusing only on the target position at the onset of the crash pulse, option (C) aims to include the entire pre-crash motion derived from the MB simulation. Hence, a small rigid part was directly attached to each landmark, shown in Fig. 7 (*right*). The motion of the rigid parts can be controlled independently via prescribed motion in translational and rotational degrees-of-freedom. The landmark velocities derived from the MB simulation were directly applied to the corresponding rigid part to move the HBM along the same path as calculated in the MB pre-crash simulation. The deletion of the fixation beams at t_0 releases the HBM from the guided rigid parts.

All FE simulations were performed using ANSYS LS-Dyna R12.2 (revision 217-gfcd6dde0c9) mpp single precision on a high-performance cluster running Debian GNU/Linux 12.14 and OpenMPI 4.1.4.

Evaluation of pre-crash kinematics and injury response

The results of the in-crash simulations were assessed using the open-source data-processing tool Dynasaur v1.3.53 [24]. In a first step, the final pose of the HBM after the pre-crash phase was compared for all three options. A measure of the accuracy with which the target coordinates were reached was defined as the resultant of the differences in all three axes between the target position from the MB simulation and the actual position reached in the FE simulation.

The second step incorporated the comparison of the in-crash behaviour across all three options. The overlay of in-crash trajectories of the landmarks gives insights into the influence of the applied positioning method. The findings drawn from the trajectory comparison were supported by the evaluation of the selected injury metrics. The following injury metrics were calculated for the in-crash phase only:

- Head injury criterion (HIC);
- The AIS2+ head injury risk based on HIC_{15} [25];
- Diffuse Axonal Multi-Axial General Evaluation (DAMAGE) MPS [26];
- DAMAGE AIS1, DAMAGE AIS2 and DAMAGE AIS4+ [27];
- Maximum principal strains and 95th percentile strains in ribs and cortical bones.

III. RESULTS

The pre-crash kinematics and injury response is compared for all three options in the following section. The findings are discussed based on a selection of results. The full set of results for both pre-crash scenarios are provided in the appendix.

Comparison of passenger pre-crash kinematics and posture at t_0

The pre-crash displacements of all landmarks measured in the FE simulation were compared to the input from the MB simulation. Comparisons of all landmarks are shown in the Appendix, in Fig. B3 and Fig. B4 for the *Brake & Steer* scenario and in Fig. C3 and Fig. C4 for the *Brake* scenario. The comparison is discussed in detail by hand of the head CoG for the *Brake & Steer* scenario for options (A) and (B) in Fig. 8 (top) and option (C) in Fig. 8 (bottom). The shown trajectories represent the displacements relative to the vehicle.

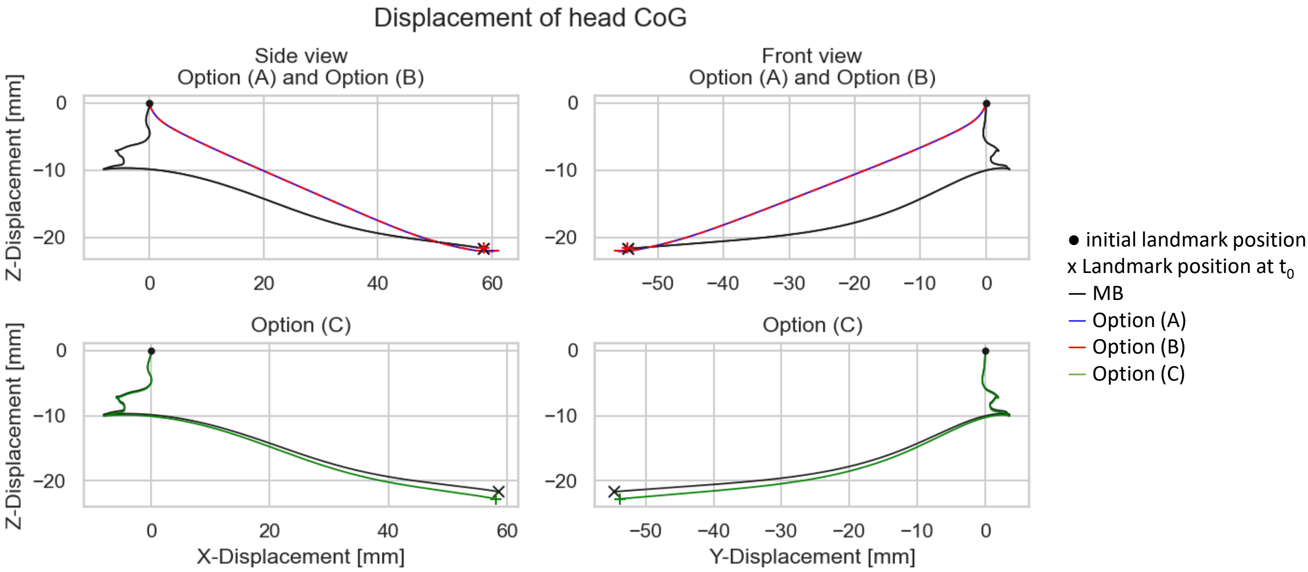

Fig. 8. Displacements of head CoG (relative to the vehicle) for options (A) and (B) (top) and option (C) (bottom) for scenario *Brake & Steer.*

Options (A) and (B) demonstrated a path-independent movement to the target position and reproduced the target Head CoG coordinates with a deviation of 0.082 mm. As option (A) and (B) only differ from the onset of the in-crash phase, the same landmark displacement is recorded in the pre-crash phase. As a result, the trajectories obtained with options (A) and (B) lie on top of each other and are visually indistinguishable in the plot. In contrast, the landmark followed the path of the pre-crash movement in option (C), where a small cumulative deviation is evident. The difference in the target position was 1.425 mm, which was the highest observed difference among all landmarks in option (C). The highest difference in option (A) and (B) was 1.317 mm, which occurred at the left radius. The deviations of all landmarks for the scenario *Brake & Steer* and *Brake* are listed in Table BI and Table CI in the Appendix.

Comparison of in-crash behaviour between all positioning options

The effect of the positioning method on the in-crash behaviour and injury response of the HBM was identified by comparing the landmark trajectories and injury metrics for all three options. Fig. 9 illustrates the trajectories, for example for the head CoG, sternum and left radius, for the *Brake & Steer* scenario.

The pre-crash phase trajectories are given in dashed lines and the in-crash phase trajectories in solid lines, coloured according to the corresponding option. The initial position is indicated with a black dot, while the positions after the pre-crash phase are indicated with an *x*.

A comparable in-crash movement of the head CoG was observed for options (B) and (C), whereas option (A) showed a different track. In contrast, the radius left trajectory was comparable between options (A) and (B) and deviated more in option (C). The sternum followed a different trajectory in all three options. As for the examples given, no clear trend was observed in the comparison of the remaining landmarks in both scenarios. Comparisons of the trajectories of all landmarks for the *Brake & Steer* and *Brake* scenarios are shown in Fig. B5 and Fig. C5 in the Appendix, respectively.

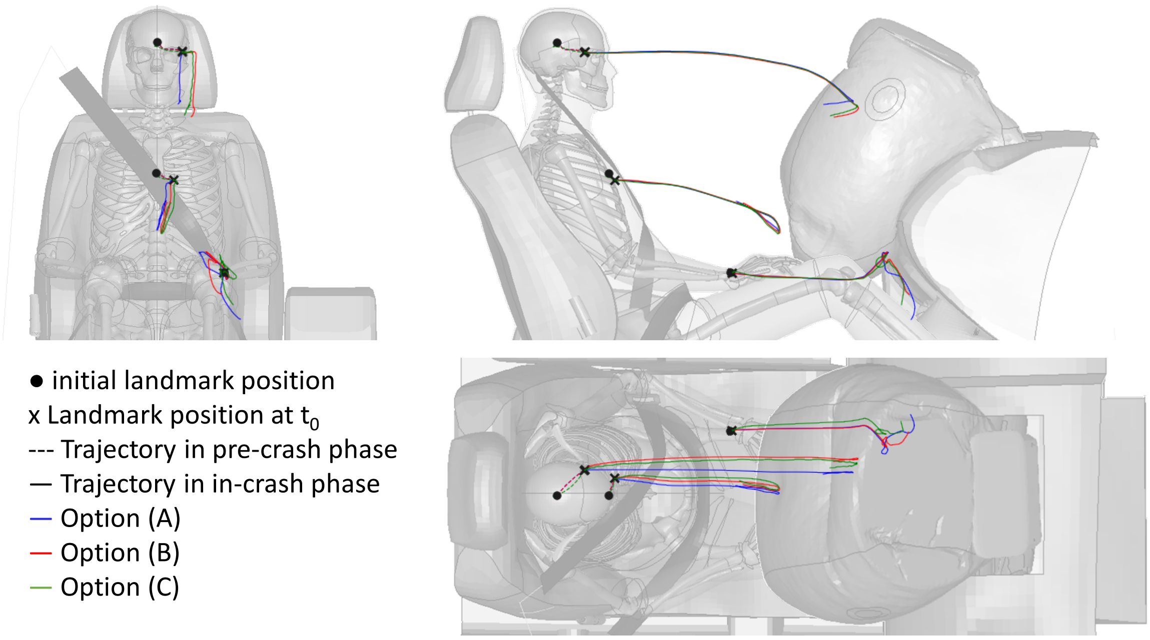

Fig. 9. Trajectories of landmarks in pre- and in-crash phases of scenario *Brake & Steer* for options (A), (B) and (C).

The injury criteria HIC, HIC AIS2+, DAMAGE MPS, DAMAGE AIS1, DAMAGE AIS2 and DAMAGE AIS4+ are listed in TABLE I for all options of both pre-crash scenarios, as well as the baseline simulation with no pre-crash (PC) phase. The relative deviation in respect to option (A) of each pre-crash scenario is noted in parentheses. No clear trend could be observed in the comparison of the HIC values and HIC-based AIS2+ injury risks. Nevertheless, two different trends for DAMAGE were observed for both pre-crash scenarios. For the *Brake & Steer* scenario, increasing values were observed in option (C), but option (B) showed the highest DAMAGE values for the *Brake* scenario.

TABLE I
INJURY CRITERIA FOR THE BASELINE (NO PRE-CRASH) AND BOTH PRE-CRASH SCENARIOS

		Brake & Steer			Brake		
	No PC	Option (A)	Option (B)	Option (C)	Option (A)	Option (B)	Option (C)
HIC	385.0	290.5	282.9 (-2.6%)	350.8 (20.8%)	298.4	289.6 (-2.9%)	270.8 (-9.2%)
HIC AIS2+	0.116	0.064	0.060 (-6.0%)	0.096 (51.6%)	0.068	0.063 (-6.7%)	0.054 (-20.4%)
DAMAGE MPS	0.602	0.554	0.551 (-0.5%)	0.616 (11.2%)	0.568	0.600 (5.6%)	0.569 (0.2%)
DAMAGE AIS1	0.955	0.978	0.976 (-0.2%)	0.997 (1.9%)	0.985	0.995 (1.0%)	0.985 (0.0%)
DAMAGE AIS2	0.933	0.861	0.857 (-0.5%)	0.947 (10.0%)	0.886	0.930 (5.0%)	0.887 (0.1%)
DAMAGE AIS4+	0.450	0.307	0.300 (-2.3%)	0.494 (60.9%)	0.346	0.442 (27.7%)	0.347 (0.3%)

The loading on the thorax during the in-crash phase of the *Brake & Steer* scenario was evaluated by analysing the rib strains, as illustrated in Fig. 10. The 95th percentile strain of each rib is coloured according to the evaluated option, with the maximum principal strains (MPS) overlaid in grey. The corresponding illustrations for the *Brake* scenario can be found in Fig. C6 in the Appendix.

The highest 95th percentile stain values were observed in the ribs R1 to R4, L1 and L5 to L8. When L1 is excluded, the strain distribution can be correlated with the loadings induced by the belt routing. The analysis of the MPS values did not show such a consensus, since high MPS values occurred in multiple ribs on both sides.

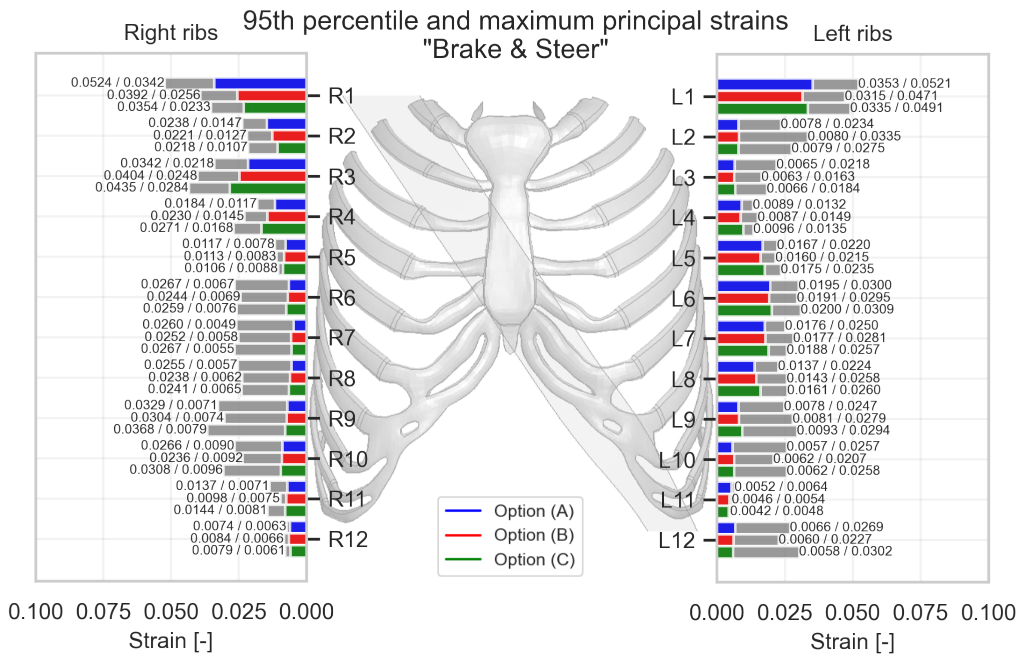

Fig. 10. The 95th percentile and maximum principal strains in the in-crash phase of scenario *Brake & Steer* for options (A), (B) and (C). Please note that the legend is positioned in the centre between the bar charts.

A similar illustration for cortical bone strains is shown in Fig. 11. Increased strains were observed for the right and left radius, the sternum and the right ulna. The corresponding illustrations for the *Brake* scenario can be found in Fig. C7 in the Appendix.

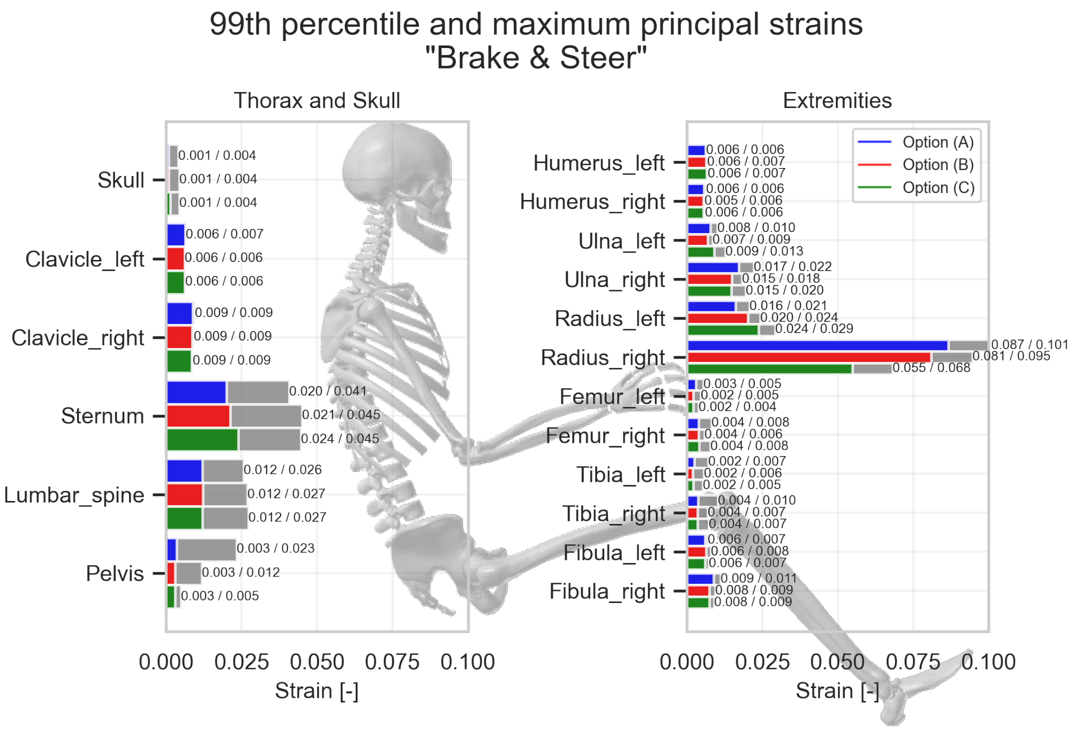

Fig. 11. Strains in cortical bones in the in-crash phase of scenario *Brake & Steer* for options (A), (B) and (C).

Comparison computational cost between all positioning options

To determine the approximate efficiency of the approaches analysed in the present study, their computational wall times (i.e., the time a simulation takes from start to termination) are listed in TABLE II. The wall times in TABLE II are based on simulations of the scenario *Brake*. However, upon investigation, the wall times for the scenario *Brake & Steer* were found to be practically identical (differences below 1%).

In addition to the three options (A), (B), and (C), a baseline simulation without pre-crash phase was also performed. This simulation had a wall time of 7 hours and 8 minutes. All three approaches had comparable wall times ranging from 17 hours and 35 minutes to 17 hours and 43 minutes, representing an increase of about 150% compared to the in-crash-only simulation.

Since the VIVA+ HBM used in the present study is not an active HBM designed for simulating long duration pre-crash manoeuvres, no direct comparison simulation spanning both pre- and in-crash phase was performed.

TABLE II
COMPUTATIONAL COST FOR ALL APPROACHES COMPARED TO THE BASELINE WITHOUT PRE-CRASH PHASE

Approach	Phase duration [ms]		Wall time [h]	Relative Increase
	Pre-crash	In-crash		
No pre-crash	0	150	7.14	0%
Option (A)	250	150	17.71	148%
Option (B)	250	150	17.82	150%
Option (C)	250	150	17.58	146%
Full FE HBM (estimate)	630	150	34.17	379%

However, to provide an estimate, the wall time equivalent of 1 ms of simulation time (during the pre-crash phase) was determined. Using this time ratio of 155 s per ms, the pre-crash duration of 630 ms and the wall time of the baseline simulation, the wall time of a simulation using a theoretical VIVA+ active HBM was approximated at 34 hours and 10 minutes.

IV. DISCUSSION

The pre-crash phase of two generic pre-crash manoeuvres was simulated with MB using an A-HBM. The pre-crash behaviour of the occupant in both scenarios was determined and transferred to the FE simulation via three different approaches, enabling the HBM posture at t_0 and the injury outcome to be compared. The pre-crash posture determined from MB simulations could be reproduced in the FE simulation to a certain degree of accuracy with all three options. Although no clear trend was observed, an effect on the in-crash trajectories and injury outcome was demonstrated.

Limitations

The results need to be interpreted in view of certain limitations that are applicable to this study. First, the influence of the positioning method was analysed based on two generic pre-crash scenarios combined with the same in-crash pulse. While the extent to which the observed effects are directly transferrable to other pre-crash scenarios was beyond the scope of the present study, the general approach can be applied to any pre-crash motion.

Although care was taken to ensure consistent occupant positioning, restraint routing, and coordinate-system transformation between the multibody and finite element environments, residual discrepancies in belt representation, contact formulation, and local tissue interaction cannot be completely excluded. These effects may influence belt preload, local deformation states, and subsequent occupant kinematics at crash initiation. However, the purpose of the workflow is not to exactly replicate belt stresses between MB and FE models, but to transfer a physically plausible pre-crash occupant state into the subsequent high-fidelity in-crash environment.

Furthermore, the simulations were conducted using a 50th percentile male HBM. Investigations including other anthropometries or sexes may lead to different occupant behaviour, as shown by [28]. Therefore, the significance of the results is limited to the prescribed boundary conditions and the selected anthropometry.

Computational cost

One common advantage of all three presented approaches is their reduced computational cost compared to using a detailed FE HBM during the pre-crash phase. While future studies could investigate if even shorter positioning phases are feasible, this was not the focus of the present study. Nevertheless, the wall time comparison showed that even for the relatively short pre-crash time of 630 ms, which was considered in this study, all three approaches reduce the wall time by about 50%. This reduction is in line with the respective reduction in simulation time.

Similarly, when comparing the estimated wall time of a simulation with a theoretical VIVA+ active HBM to the wall times of the three approaches, the wall time ratio (1.92-1.94) and simulation time ratio (1.95) follow almost a perfect 1:1 relationship. In essence, this means that the computational cost benefits would increase for increased pre-crash durations.

***Differences in landmark positions at* t_0**

The target positions of the landmarks after the pre-crash phase were reproduced with minor deviations in all three options. Investigations into the cause of the deviations in positioning options (A) and (B) revealed that some positioning beams had not fully compressed during the pre-crash phase. This behaviour was observed for the landmarks on both knees, the left heel and the left radius. Specifically, remaining beam length when comparing the MB and FE target positions, the deviations decreased to a maximum of 0.776 mm for scenario *Brake & Steer* and 0.523 mm for scenario *Brake*. These incomplete beam compressions indicate that the available pre-crash duration may not be sufficient to achieve a fully converged HBM positioning state or that the beam forces would need to be increased for these landmarks. Given the small magnitude (below 1 mm) of these deviations however, it seems unlikely that the observed response differences originate from residual positioning effects rather than solely from the investigated positioning methodology.

Landmarks positioned with option (C) follow the exact velocity path gained from MB simulations. Nonetheless, a difference increasing over time is observed, indicating a cumulative error. Upon further investigation it was determined that this increasing difference can be attributed to the inherently different behaviour of the MB and FE models. While the geometries were aligned in the initial state, a difference in response during the dynamic positioning phase is to be expected. Yet, the maximum observed difference across all landmarks and options is less than 1.5 mm. When compared to the distance covered by each landmark, the relative deviation is less than 3.3%. Only for the left radius, the relative deviation is 23%. When considering the covered distance of only 5.56 mm, the difference of 1.317 mm is relatively high. However, as with the residual differences observed in the positioning beams used in options (A) and (B), it seems unlikely that positioning differences below 2 mm would have a meaningful effect on overall in-crash kinematics, on subsequent injury criteria values or injury risks.

Influence of the positioning option

Despite observing differences in in-crash kinematics and injury criteria when comparing the three options for both scenarios, no clear trend could be established. Whether the in-crash trajectory of a landmark differs between all options or is comparable within some options remains inconclusive. The loadings induced by the belt are reflected by the strains measured in the ribs, however, no clear statement on the influence on the positioning method can be made. Increased strains were observed in the right radius in the pre-crash scenario *Brake & Steer*, which can be attributed to the different load path due to the lateral movement in the pre-crash phase. Investigating strain values from all cortical bones, no clear trend between the options was observed. Although a trend was observed in the DAMAGE values, the direction of the trend differed between the two scenarios. For the *Brake* scenario, option (B) shows the highest DAMAGE values, whereas option (C) shows the highest DAMAGE values for the *Brake & Steer* scenario. As DAMAGE uses rotational head kinematics to estimate the maximum strain in the brain, option (C) seems favourable as it preserves these kinematics most accurately. The increased DAMAGE values observed with option (B) compared to option (C) in the *Brake* scenario, could also be the result of the A-HBMs pre-crash motion actively reducing the head rotation prior to head-airbag interaction and, as a result, the head rotational dynamics responsible for increased DAMAGE values, i.e., and brain strains.

In terms of injury criteria, the baseline simulation, which did not consider any pre-crash motion, yielded comparable results to all three approaches. This is to be expected to a certain degree, considering that the same crash loads were applied and the position differences and relative velocities where below 60 mm and 0.6 m/s respectively. However, it can safely be assumed that a more noticeable effect would be observed with pre-crash scenarios resulting in higher forward displacements and higher relative velocities at t_0. The limited forward displacements and relative velocities observed in both investigated scenarios can be attributed to two circumstances:

First, the length of the pre-crash pulse, and therefore the time at which the in-crash pulse begins, was determined based on the moment at which the HBM's relative velocity to the vehicle was at its maximum for the certain pulse. This definition was intended to enhance the demonstrated effect of applying time-history-based prescribed velocities in the pre-crash phase. The negative impact was that the absolute forward displacement decreased compared to if the pre-crash manoeuvre had been continued for longer before the crash occurred.

Second, since the pre-crash simulations were conducted with an A-HBM counteracting forward deflections via muscle control, relative velocities did not exceed 0.6 m/s at t_0, which also limited the HBM's deflection. The effect of different levels of muscle activity in the pre-crash phase on the applied positioning options remains to be determined.

Benefits of the developed approach

Commonly used HBM positioning methods focus on replicating the posture and/or initial velocities at t_0. Landmarks are dragged along a direct trajectory to the desired target position. In contrast, this novel approach guides landmarks along the same path as that determined in the pre-crash simulation. Furthermore, although the computational cost benefits are preserved and the same landmark positions are reached as with conventional methods, different injury outcomes are observed due to the different t_0 kinematics. When limited effects are observed, it is assumed that the novel approach generates a more accurate representation of HBM conditions at t_0. This is of particular interest when considering complex pre-crash manoeuvres involving not only constant steering and braking pulses, but also diverse lateral accelerations.

V. CONCLUSION

A novel approach to transfer the posture and kinematics from pre-crash to in-crash simulation was developed. The in-crash trajectories and injury metrics from the novel positioning method were compared to those from commonly used approaches and the effects were highlighted. Although no clear trend between the options applied could be identified, influences on the injury outcome could be demonstrated. The benefit of representing the t_0 kinematics more accurately with the novel approach may take on even greater significance in complex pre-crash characteristics.

VI. ACKNOWLEDGEMENTS

The authors gratefully acknowledge the IT Services (ZID) of Graz University of Technology, Austria, for providing access to high-performance computing resources.

This work was carried out by the Vehicle Safety Institute of Graz University of Technology and the Institute of Engineering and Computational Mechanics at the University of Stuttgart within the research project Safe-X, a Tech Center i-protect project. This document reflects only the authors' view; the funding organisations are not responsible in any way for any use that may be made of the information it contains.

AI Disclosure: Artificial Intelligence-based tools were used to assist with language refinement (DeepL web application, Responsible AI platform University of Stuttgart OpenAI GPT 5.1 Oct. 2025) and drafting of code snippets for the Python-based injury assessment (GitHub Copilot version 1.372.0). The authors critically reviewed and edited all AI-assisted content and remain fully responsible for the originality, accuracy, and scientific validity of the submission.

VII. REFERENCES

[1] Hu, J., Lin, Y.-S., Boyle, K., & Reed, M.: Parametric Model for Simulating Occupant Responses During Pre-Crash Vehicle Maneuvers. National Highway Traffic Safety Administration, **2025**(Report No. DOT HS 813 632).

[2] Matsuda, T.; Yamada, K.; Hayashi, S.; Kitagawa, Y. (2018): Simulation of Occupant Posture Changes due to Evasive Manoeuvres and Injury Predictions in Vehicle Frontal and Side Collisions. IRCOBI Conference. International Research Council on the Biomechanics of Injury. 12.-14.9.2018. Athens, Greece.

[3] Östmann, M.; Jakobsson, L. (2016): An Examination of Pre-crash Braking Influence on Occupant Crash Response using an Active Human Body Model. IRCOBI Conference. 14.-16.09.2016. Malaga, Spain.

[4] Dahiya, A.; Untaroiu, C. (2023): Influence of Pre-Crash Vehicle Maneuvers on Front Passenger Safety Performance Response. SAE International Journal of Transportation Safety, **11**(2): 263–272.

[5] Dahiya, A.; Untaroiu, C. (2025): The Influence of Occupant Characteristics, Seat Positioning, and Pre-Crash Maneuvers on Front Passenger Safety Performance. Journal of Biomechanical Engineering, **147**(3).

[6] Iraeus, J.; Mishra, E.; Östh, J. (2023): Comparison of Average Female and Male Active HBM Responses in Whole-Sequence Frontal Crash Simulations. IRCOBI Conference. International Research Council on the Biomechanics of Injury. 13.-15.09.2023. Cambridge, UK.

[7] Yamada, K.; Gotoh, M.; Kitagawa, Y.; Yasuki, T. (2016): Simulation of Occupant Posture Change during Autonomous Emergency Braking and Occupant Kinematics in Frontal Collision. IRCOBI Conference. 14.-16.09.2016. Malaga, Spain.

[8] Hay, J. (2022): *A Surrogate Model-enhanced Simulation Framework for Safety Performance Assessment of Integrated Vehicle Safety Systems*, *Shaker Verlag*, Aachen.

[9] Bechler, F.; Fehr, J.; Neininger, F.; Knöß, S.; Grotz, B. (2023): Combining Knowledge and Information - Graph-Based Description of Driving Scenarios to Enable Holistic Vehicle Safety. International Technical Conference on the Enhanced Safety of Vehicles. 3-6 April 2023. Yokohama, Japan.

[10] Hay, J.; Schories, L. et al. (2023): Application of Data-driven Surrogate Models for Active Human Model Response Prediction and Restraint System Optimization. Frontiers in Applied Mathematics and Statistics, **9**.

[11] Öztürk, A.; Mayer, C. et al. (2019): A Step Towards Integrated Safety Simulation through Pre-Crash to In-Crash Data Transfer. International Technical Conference on the Enhanced Safety of Vehicles. 10-13 June. Eindhoven, Netherlands.

[12] Breitfuß, D.; Klein, C.; Lancashire, R.; Bosma, F.; Pucher, J.; Leitgeb, W. (2022): Solver- and Model-Agnostic Method to Transfer Pre-Crash Occupant Kinematics to an In-Crash Occupant Model for Continuous Occupant Assessment. IRCOBI Conference. International Research Council on the Biomechanics of Injury. 14.-16.09.2022. Porto, Portugal.

[13] Steffan, H. (1993): PC-CRASH, A Simulation Program for Car Accidents. ISATA. 13.-17.September 1993. Aachen.

[14] Vehicle Safety Institute (2020): CEDATU - Central Database for In-Depth Accident Study, https://www.tugraz.at/en/institutes/vsi/research/vsi-tools/accident-database/general-information.

[15] vufo (2018): GIDAS, URL: http://www.vufo.de/forschung-und-entwicklung/gidas/.

[16] Siemens Industry Software and Services BV (SSIS). (2020) *Simcenter Madymo Model Manual, Version 2020.1.*, Rijswijk, Netherlands.

[17] Gstrein, G.; Leo, C.; Erlinger, N.; Kofler, D.; Jauernig, A. D.; Klug, C. (2025): Occupant response during autonomous braking manoeuvres in novel seating positions. IRCOBI Conference. International Research Council on the Biomechanics of Injury. 10.-12.09.2025. Vilnius, Lithuania.

[18] Diederich, A.; Bastien, C.; Ekambaram, K.; Wilson, A. (2021): Occupant pre-crash kinematics in rotated seat arrangements. Proceedings of the Institution of Mechanical Engineers, Part D: Journal of Automobile Engineering, **235**(10-11): 2818–2842.

[19] Lynch, K. M.; Park, F. C. (2024): *Modern Robotics: Mechanics, Planning, and Control*, *Cambridge University Press*, Cambridge, UK.

[20] Boyle, K.; Hu, J.; Reed, M. P.; Rupp, J. D. (2024): Development of Parametric Finite Element Vehicle and Restraint Models for Occupant Protection Research. IRCOBI Conference. International Research Council on the Biomechanics of Injury. 11.-13.9. Stockholm, Sweden.

[21] Iraeus, J.; Lindquist, M. (2015): Pulse shape analysis and data reduction of real-life frontal crashes with modern passenger cars. International Journal of Crashworthiness, **20**(6): 535–546.

[22] John, J.; Klug, C.; Kranjec, M.; Svenning, E.; Iraeus, J. (2022): Hello, world! VIVA+: A human body model lineup to evaluate sex-differences in crash protection. Frontiers in bioengineering and biotechnology, **10**.

[23] John, J.; Klug, C.; Kranjec, M.; Svenning, E.; Iraeus, J. (2025) *VIVA+ Human Body Model v2.0.2*.

[24] Schachner, M.; Micorek, J.; Luttenberger, P.; Greiml, R.; Klug, C.; Rajinovic, S. (2022): Dynasaur - Dynamic simulation analysis of numerical results, https://gitlab.com/VSI-TUGraz/Dynasaur.

[25] Hertz, E. (1993): A note on the head injury criterion (HIC) as a predictor of the risk of skull fracture. American Association for Automotive Medicine Annual Conference. American Association for Automotive Medicine. 1993. San Antonio, Texas.

[26] Gabler, L. F.; Crandall, J. R.; Panzer, M. B. (2019): Development of a Second-Order System for Rapid Estimation of Maximum Brain Strain. Annals of Biomedical Engineering, **47**(9): 1971–1981.

[27] Wu, T.; Sato, F. et al. (2022): Integrating Human and Nonhuman Primate Data to Estimate Human Tolerances for Traumatic Brain Injury. Journal of Biomechanical Engineering, **144**(7).

[28] Hu, J.; Fanta, A.; Neal, M. O.; Reed; Wang, J.-T. (2016): Vehicle Crash Simulations with Morphed GHBMC Human Models of Different Stature, BMI, and Age.

VIII. APPENDIX

Appendix A: In-crash pulse data

TABLE AI
PARAMETER FOR IN-CRASH PULSE

DV (delta v in km/h)	61
DUR (pulse duration in ms)	90
PDOF_H (principal direction of force – horizontal in degrees)	0.01
PDOF_V (principal direction of force – vertical in degrees)	0.01
EV1 (Eigenvalue 1)	-0.9720
EV2 (Eigenvalue 2)	-0.7300
EV3 (Eigenvalue 3)	-0.0509
EV4 (Eigenvalue 4)	0.0000
EV6 (Eigenvalue 6)	-0.0480
Yaw (angular velocity in (deg./ms)	0.0000
Pitch (angular velocity in (deg./ms)	0.0000
Roll (angular velocity in (deg./ms)	0.0000

Appendix B: Simulations results – Pre-crash phase – Scenario *Brake & Steer*

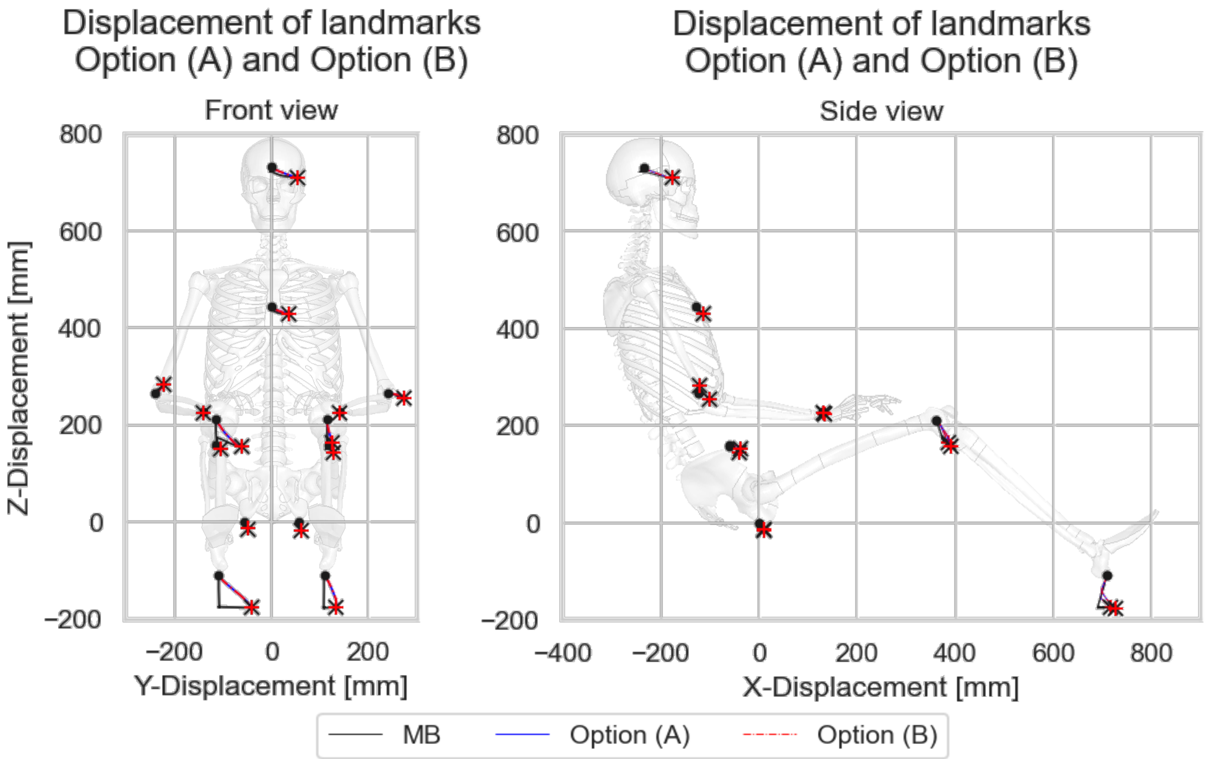

Fig. B1. Comparison of pre-crash landmark coordinates between MB and FE for option (A) and option (B) for scenario *Brake & Steer* in the side and front view.

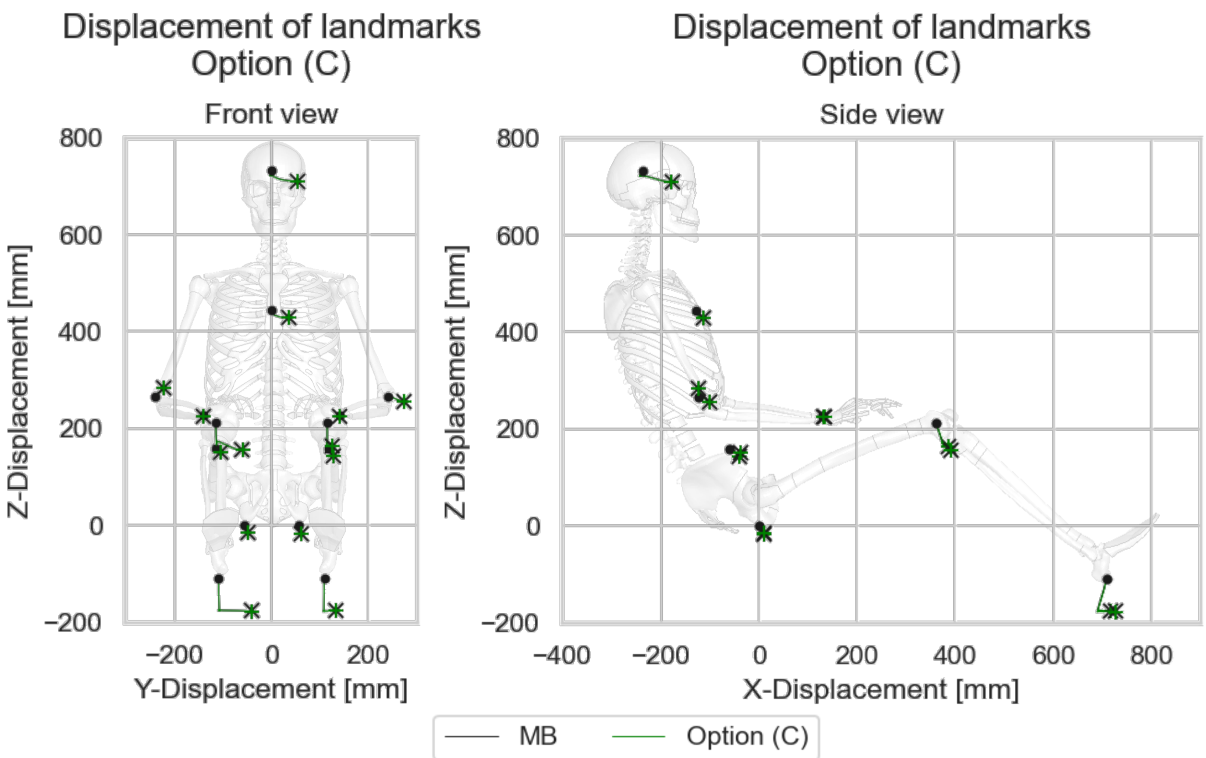

Fig. B2. Comparison of pre-crash landmark coordinates between MB and FE for option (C) for scenario *Brake & Steer* in the side and front view.

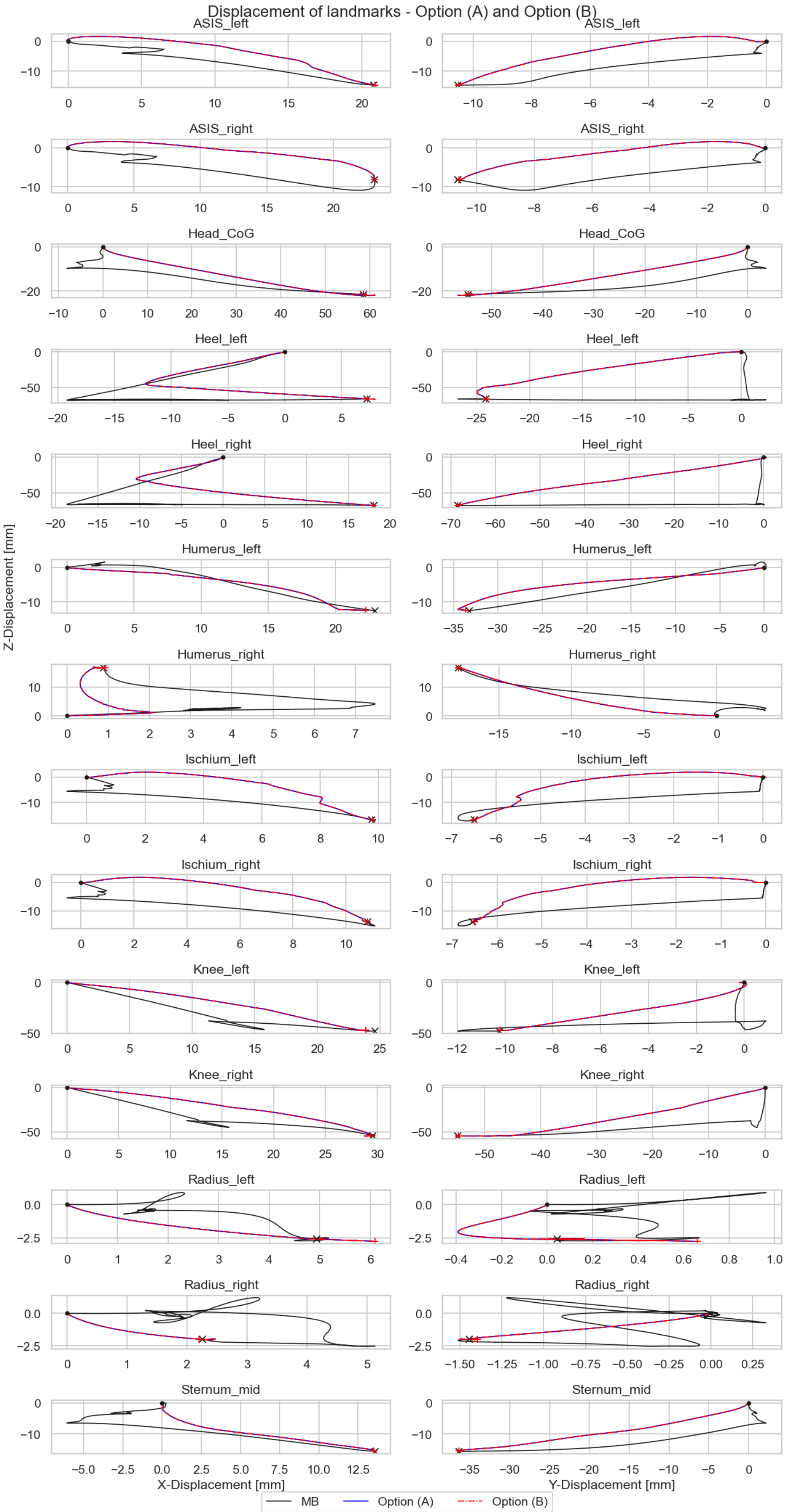

Fig. B3. Comparison of pre-crash landmark displacement between MB and FE for option (A) and option (B) for scenario *Brake & Steer* for individual landmarks.

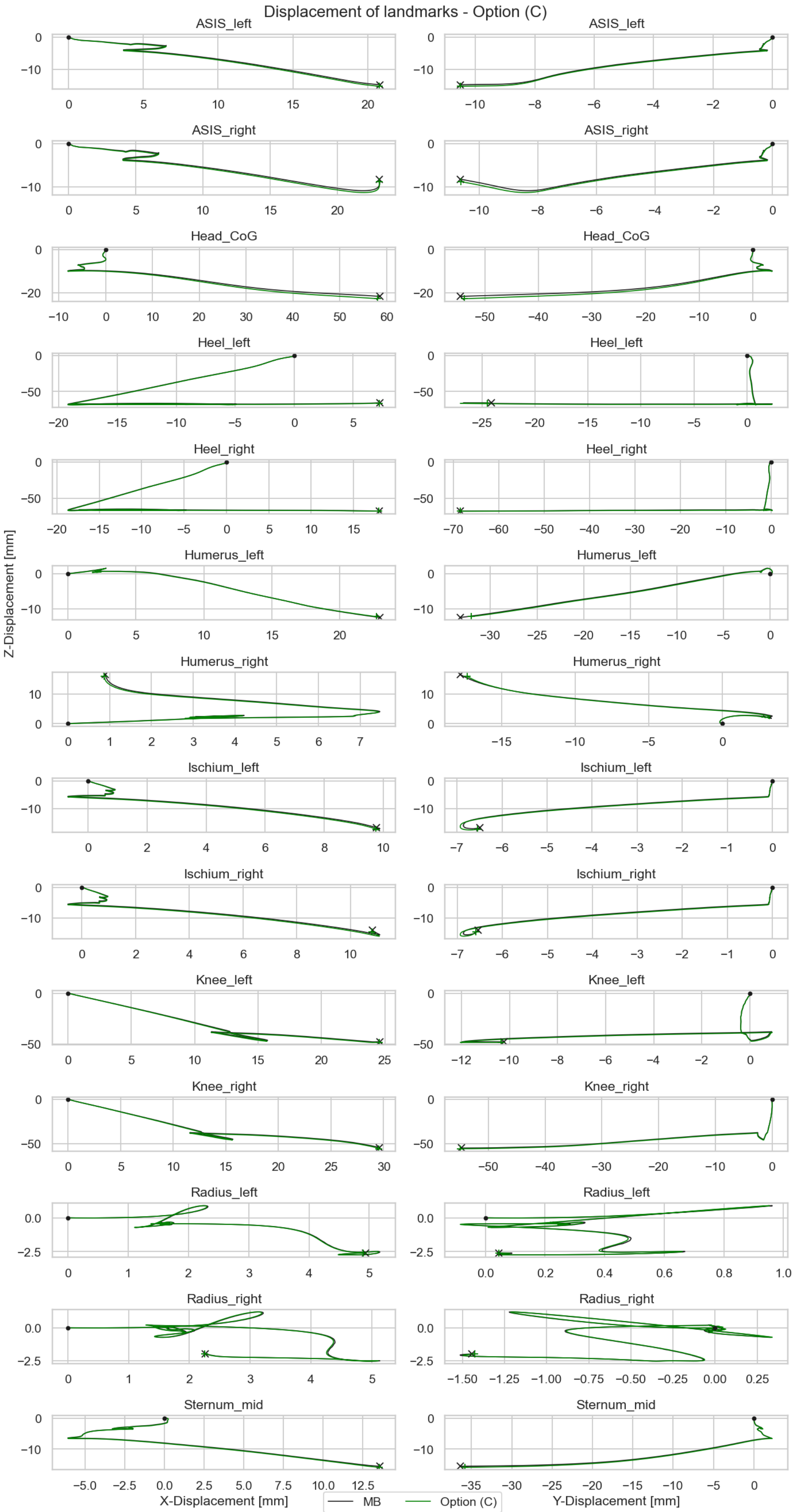

Fig. B4. Comparison of pre-crash landmark displacement between MB and FE for option (C) for scenario *Brake & Steer* for individual landmarks.

TABLE BI
DEVIATIONS OF LANDMARKS BETWEEN MB AND FE AT T_0 FOR SCENARIO *BRAKE & STEER*

Landmark	Deviations in options (A) and (B) [mm]	Deviations in option (C) [mm]
Left ASIS	0.115	0.477
Right ASIS	0.066	0.564
Head CoG	0.082	1.425
Left Heel	0.055	0.500
Right Heel	0.049	0.253
Left Humerus	0.799	1.215
Right Humerus	0.018	0.786
Left Ischium	0.044	0.502
Right Ischium	0.054	0.541
Left Knee	1.087	0.550
Right Knee	0.330	0.793
Left Radius	1.317	0.038
Right Radius	0.076	0.023
Sternum	0.113	0.702

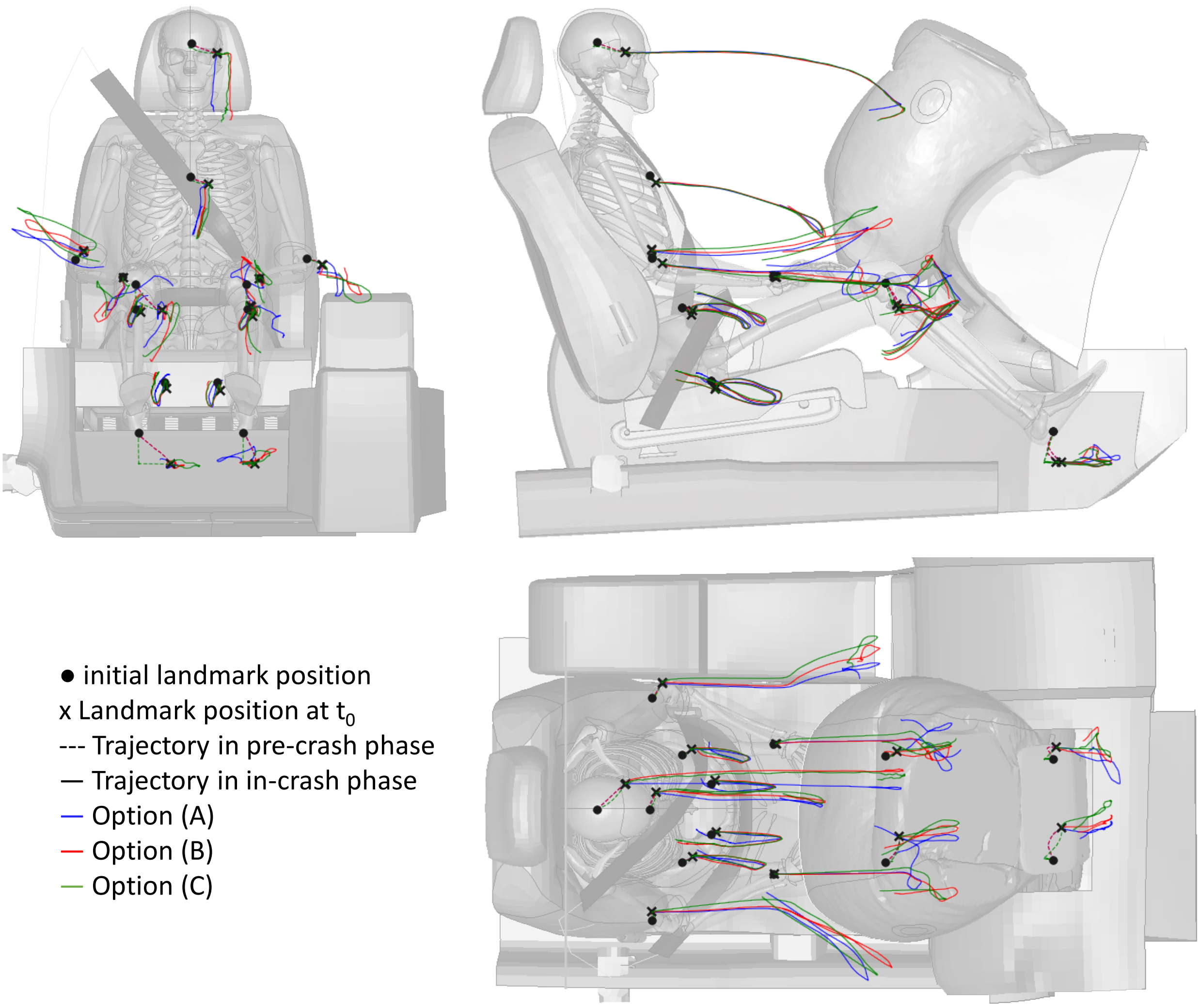

Fig. B5. Trajectories of landmarks in pre- and in-crash phases of scenario *Brake & Steer* for options (A), (B) and (C).

Appendix C: Simulations results – Pre-crash phase – Scenario *Brake*

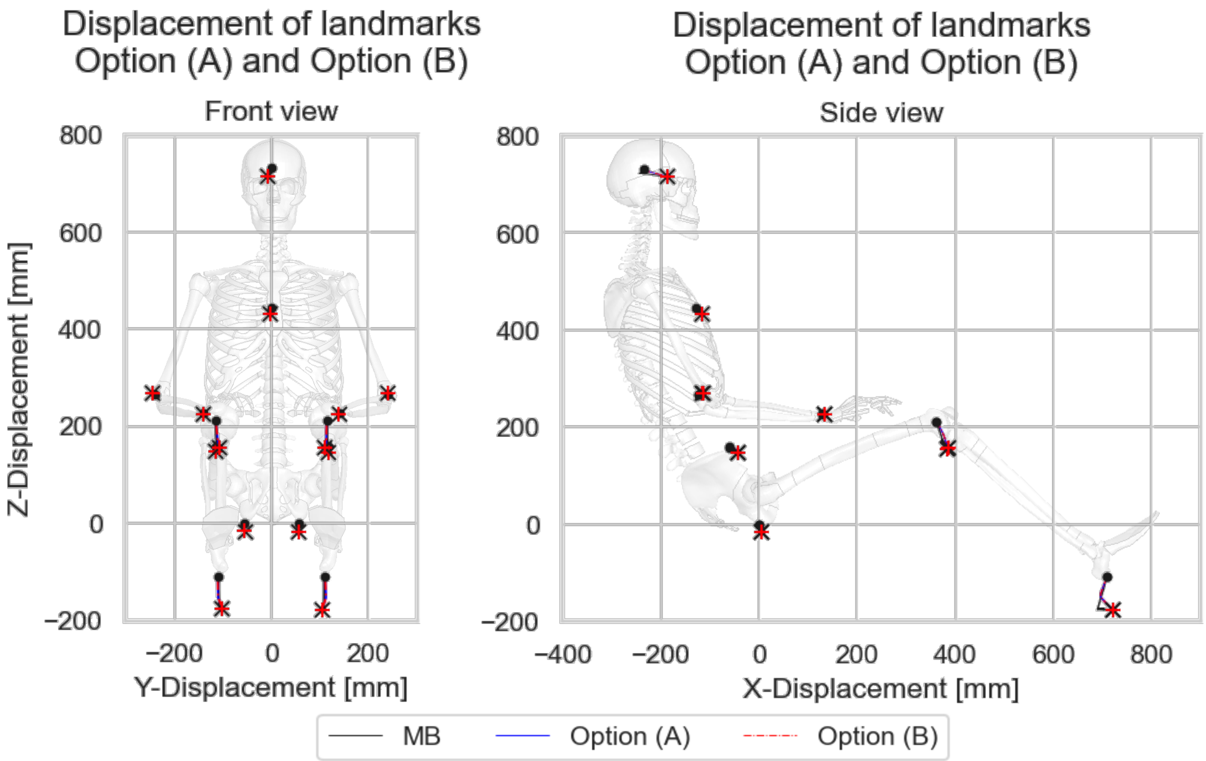

Fig. C1. Comparison of pre-crash landmark coordinates between MB and FE for option (A) and option (B) for scenario *Brake* in the side and front view.

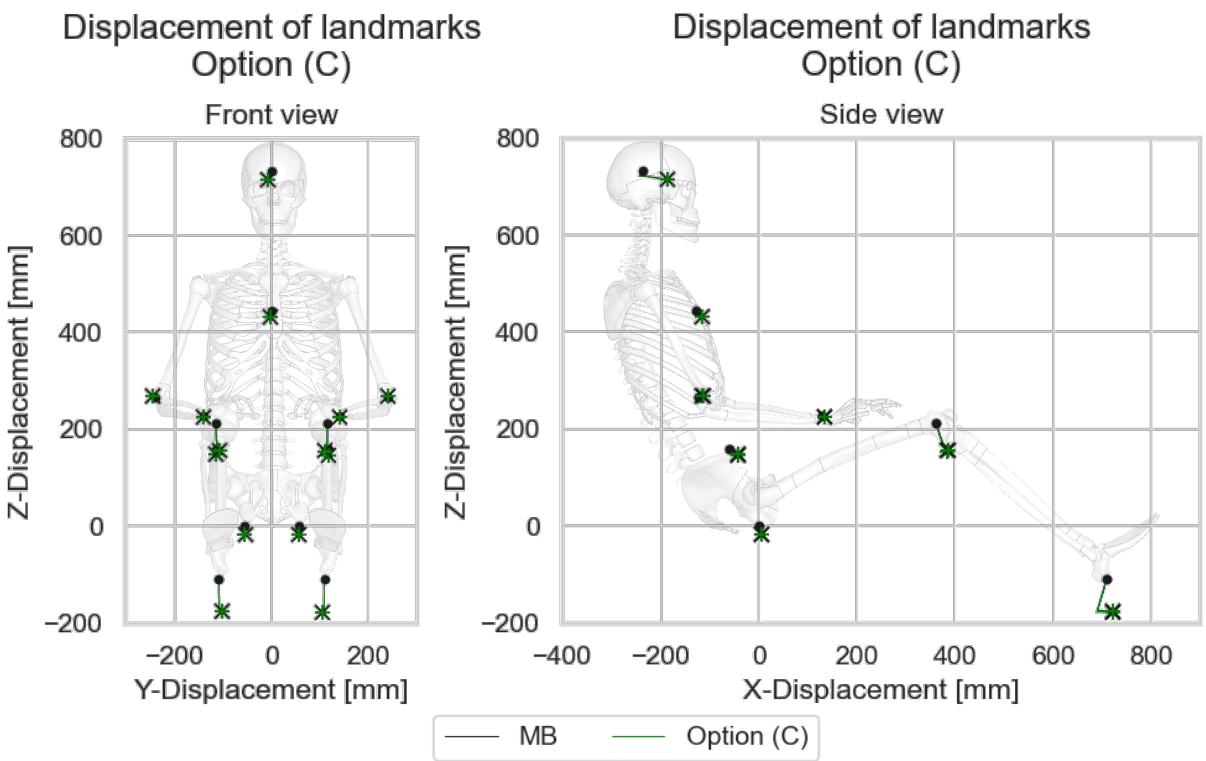

Fig. C2. Comparison of pre-crash landmark coordinates between MB and FE for option (C) for scenario *Brake* in the side and front view.

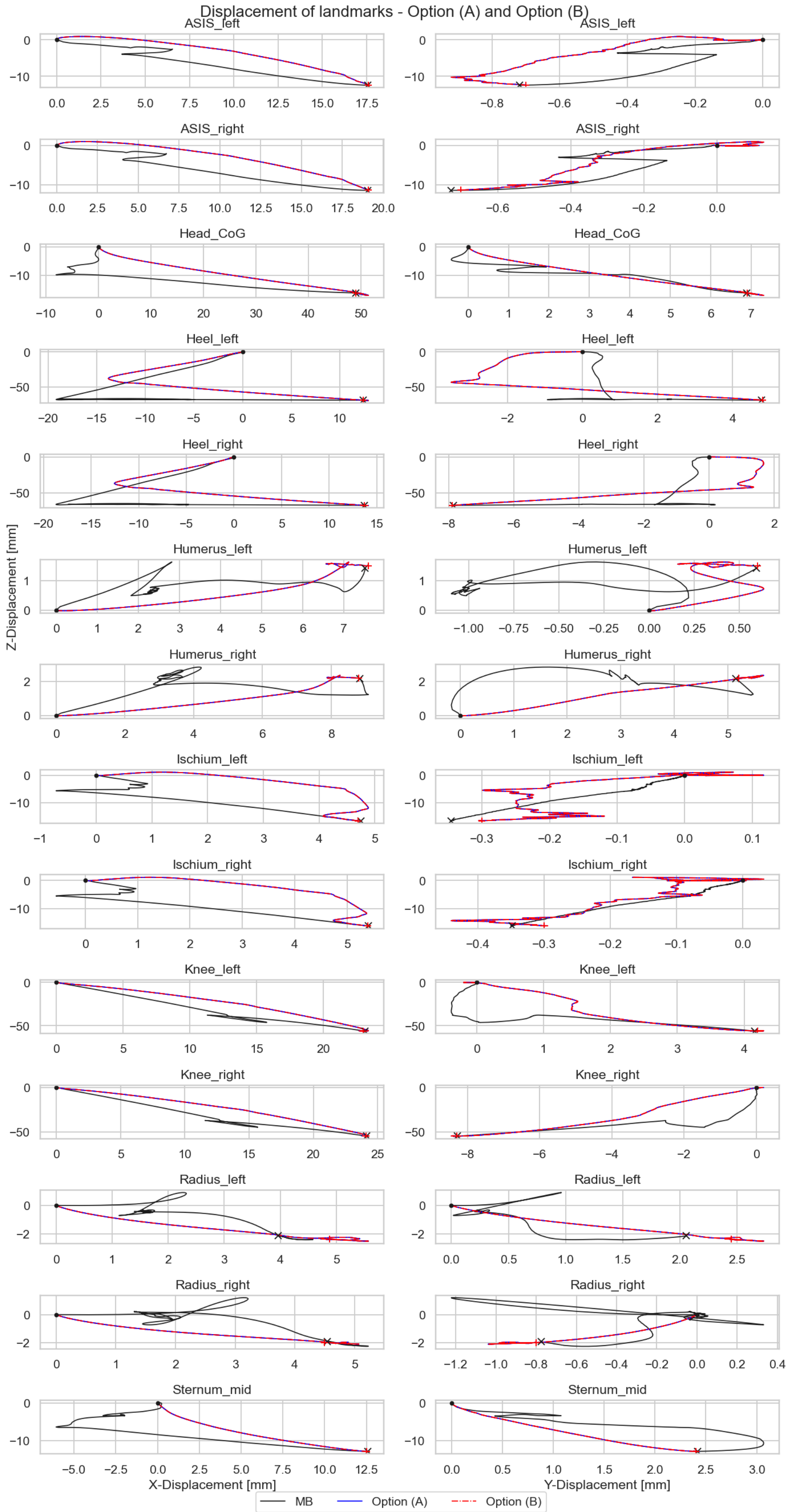

Fig. C3. Comparison of pre-crash landmark displacement between MB and FE for option (A) and option (B) for scenario *Brake* for individual landmarks.

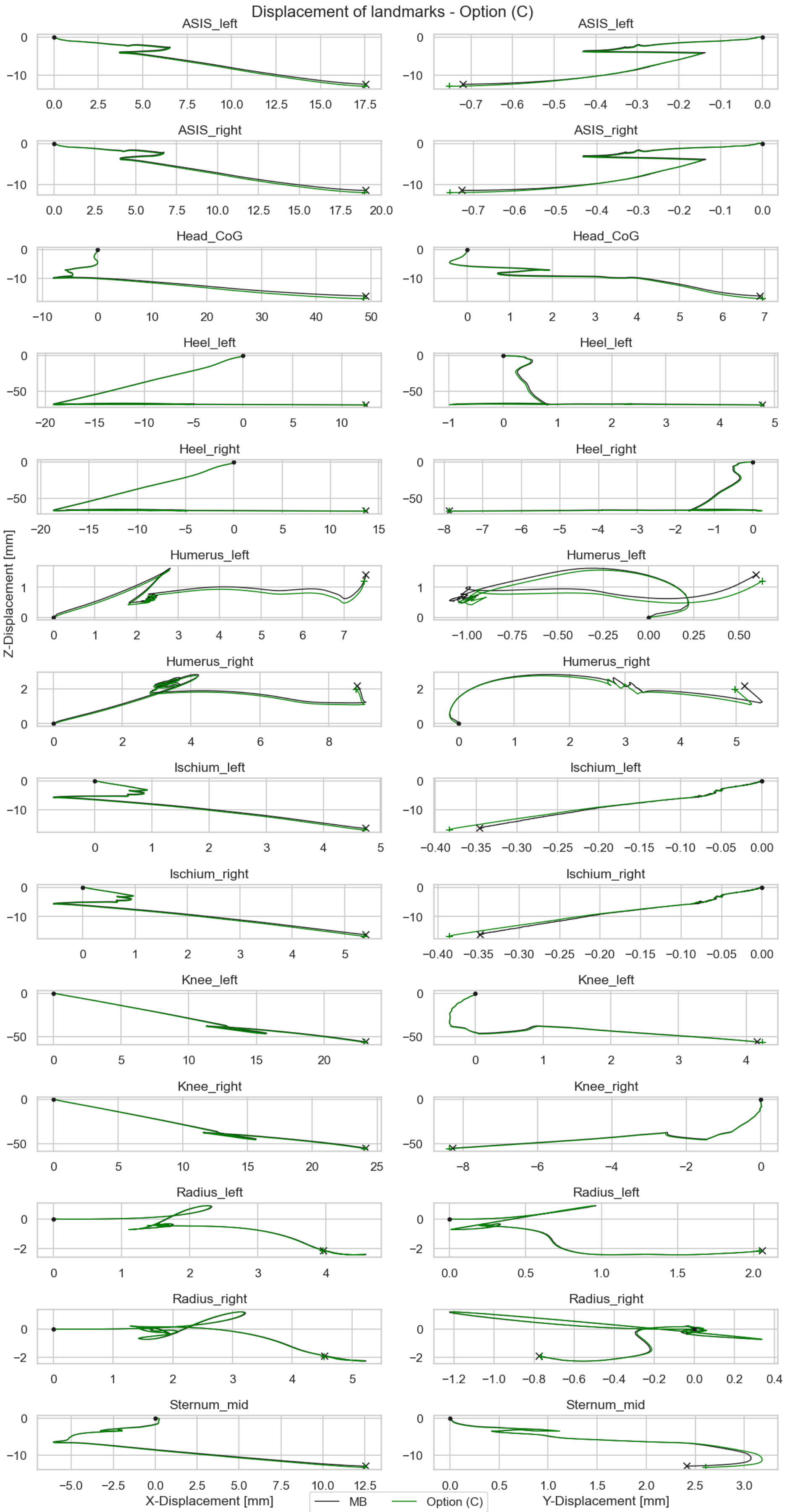

Fig. C4. Comparison of pre-crash landmark displacement between MB and FE for option (C) for scenario *Brake* for individual landmarks.

TABLE CI
DEVIATIONS IN MM OF LANDMARKS BETWEEN MB AND FE AT T_0 FOR SCENARIO *BRAKE*

Landmark	Deviations in options (A) and (B) [mm]	Deviations in option (C) [mm]
Left ASIS	0.086	0.543
Right ASIS	0.073	0.548
Head CoG	0.030	1.060
Left Heel	0.056	0.283
Right Heel	0.044	0.295
Left Humerus	0.114	0.215
Right Humerus	0.059	0.255
Left Ischium	0.067	0.531
Right Ischium	0.055	0.533
Left Knee	0.137	0.610
Right Knee	0.071	0.616
Left Radius	1.019	0.022
Right Radius	0.085	0.021
Sternum	0.071	0.409

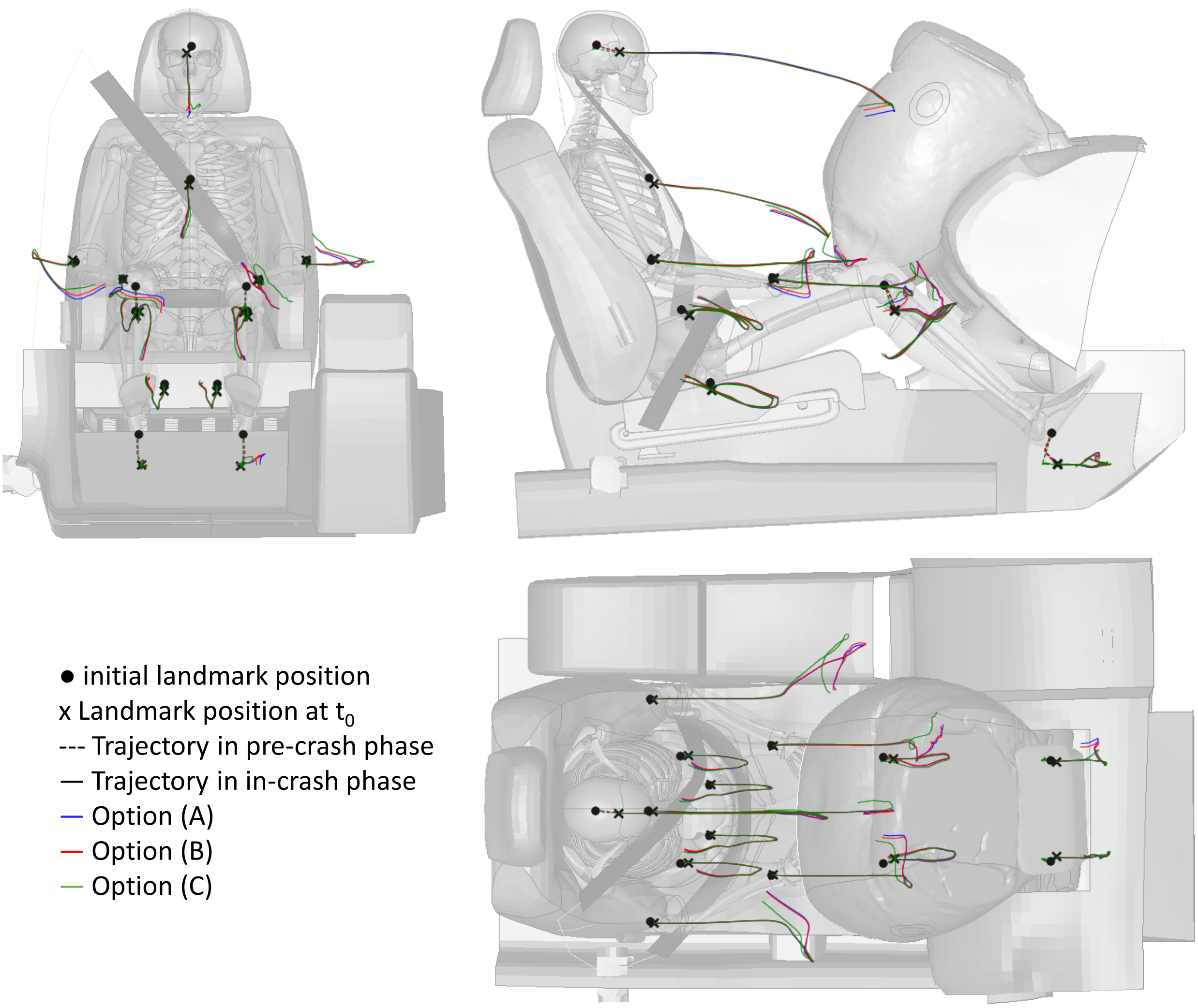

Fig. C5. Trajectories of landmarks in pre- and in-crash phases of scenario *Brake* for options (A), (B) and (C).

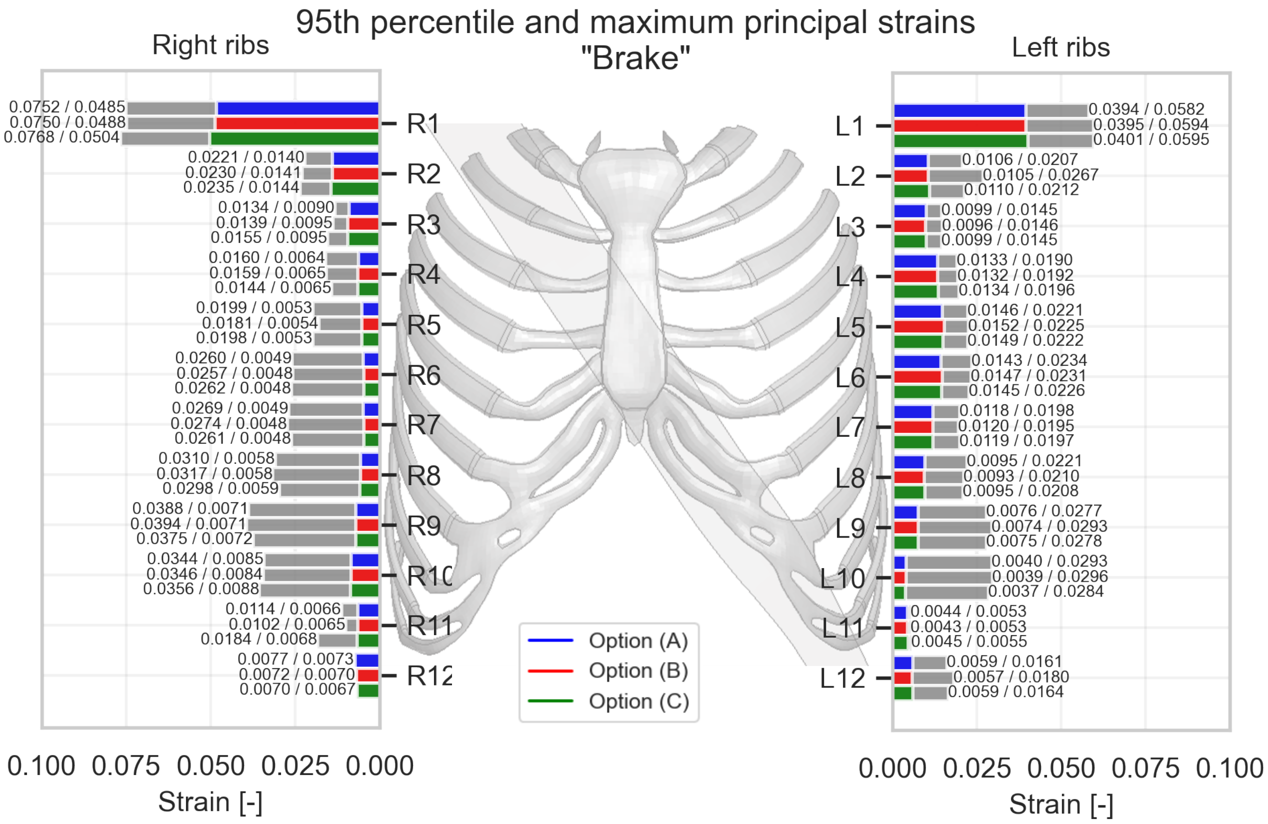

Fig. C6. Rib 95th percentile and maximum principal strains during the in-crash phase of scenario *Brake* for options (A), (B) and (C).

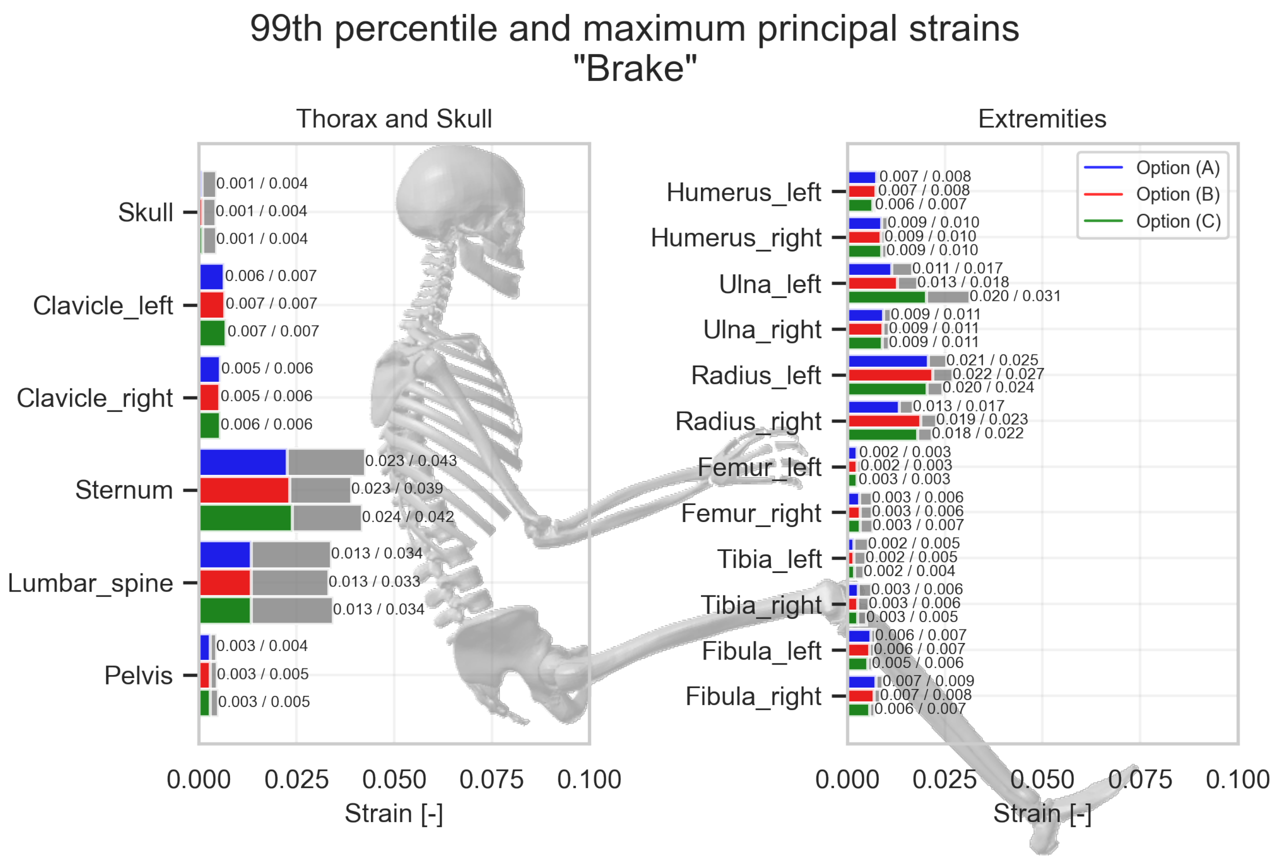

Fig. C7. Cortical bone 95th percentile and maximum principal strains during the in-crash phase of scenario *Brake* for options (A), (B) and (C).

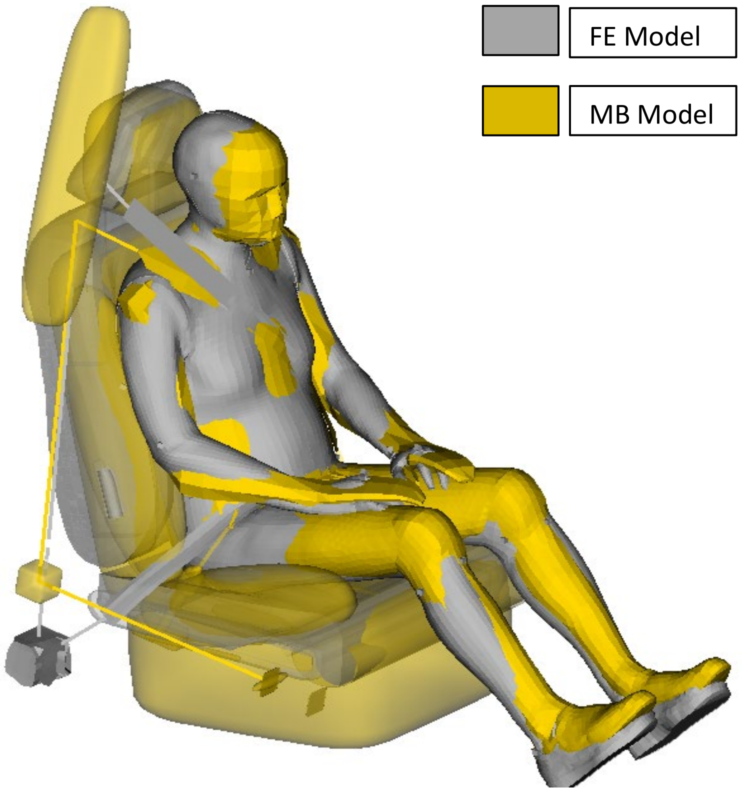

Fig. C8. MB and FE model overlapped at H-Point.

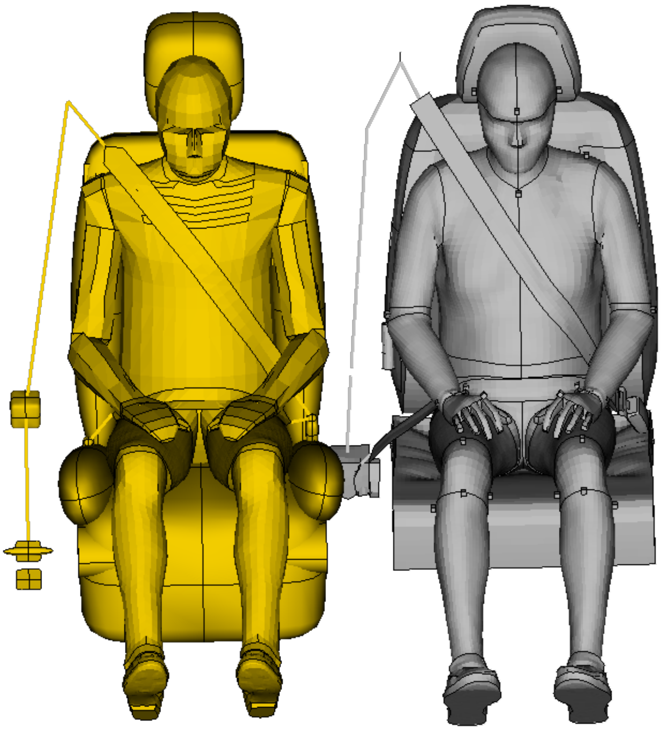

Fig. C9. Front view of MB and FE Model.